The Dissertation Committee for Daniel E. Lalich Certifies that this is the approved version of the following dissertation:

Using Radar Reflectivity To Unlock The Climate Record Contained In The Martian North Polar Layered Deposits

Committee:

John W. Holt, Supervisor

Joseph Levy

Cyril Grima

Ginny Catania

Gary Kocurek

Using Radar Reflectivity To Unlock The Climate Record Contained In The Martian North Polar Layered Deposits

by

Daniel E. Lalich

Dissertation

Presented to the Faculty of the Graduate School of

The University of Texas at Austin

in Partial Fulfillment

of the Requirements

for the Degree of

Doctor of Philosophy

The University of Texas at Austin

August 2017

Acknowledgements

Many people and organizations contributed to this work. NASA provided generous financial support through grant NNX15AM52G and an NESSF fellowship, which was supplemented by the Jackson School of Geoscience. I would like to thank my advisor, Jack Holt, for suggesting an interesting problem to work on and for giving me the freedom to approach it how I saw fit. I also want to thank Joe MacGregor, who helped me develop many of the technical skills without which this project would not have been possible, and who provided the seed for what would become a central part of my work. I want to recognize the support staff at the Jackson School and UTIG as well, especially Philip Guerrero, who always made sure my paperwork got in on time and provided so many breakfast tacos.

Many friends and fellow students also had a hand in this project, from Isaac Smith and Charles Brothers, who taught me the ropes when I first started out, to Stefano Nerozzi, Ben Cardenas, Eric Petersen, and Cassie Stuurman, who were valuable not only for their feedback but also for taking my mind off of work from time to time. I would like to thank Hope Miller in particular for her constant support, without which this project would never have been completed. Lastly, I want to thank my parents Mick and Nina, for providing me with the desire and opportunity to pursue a lifetime of learning.

Using Radar Reflectivity To Unlock The Climate Record Contained In The Martian North Polar Layered Deposits

Daniel E. Lalich, Ph.D.

The University of Texas at Austin, 2017

Supervisor: John W. Holt

The North Polar Layered Deposits of Mars are a formation of water ice ~1000 km across and ~2 km thick. For years, scientists have looked to these layers of ice and dust as a possible source of information regarding how the planet's climate has changed over the past ~4 million years. However, connecting these layers to specific climate conditions remains a challenge. Previous research has attempted to tie both radar stratigraphy and outcrop stratigraphy to the orbital cycles of Mars, but the proposed relationships are often contradictory, and struggle identify how specific layer properties might be tied to ancient climate.

To help resolve these issues, I synthesized a combination of radar data, imagery, topography, and electromagnetic modeling in an effort to quantify layer properties such as thickness and composition, and connect those properties to past climate conditions. I was able to quantitatively show that a set of layers known as marker beds is likely responsible for causing radar reflectors, and was able to show how radar reflectors could be used to infer the composition and relative thickness of these layers throughout the polar cap. With this information in hand, scientists can, for the first time, begin to realize the full potential of the North Polar Layered Deposits as a global climate record of Mars.

Table of Contents

List of Tables ... vii

List of Figures ... viii

INTRODUCTION ... 1

Chapter 1: New Martian Climate Constraints From Radar Reflectivity Within The North Polar Layered Deposits ... 4

- Introduction ... 4
- Data and Methods ... 6
- Results ... 11
- Discussion ... 14
- Conclusion ... 18

Chapter 2: Icy Dust or Dusty Ice? Radar Reflectivity as a Proxy for the Dust Content of Individual Layers in the Martian North Polar Layered Deposits ... 20

- Introduction ... 20
- Background ... 21
- Data and Methods ... 27
- Results and Discussion ... 37
- Conclusion ... 48

Chapter 3: Connecting Visible and Radar Stratigraphy in the Martian North Polar Layered Deposits ... 50

- Introduction ... 50
- Data and Methods ... 55
- Results and Discussion ... 61
- Conclusion ... 79

CONCLUSION ... 81

References ... 83

List of Tables

Table 2.1 41

Table 3.1 64

Table 3.2 69

Table 3.3 72

List of Figures

Figure 1.1 7
Figure 1.2 9
Figure 1.3 12
Figure 1.4 13
Figure 1.5 15
Figure 1.6 18
Figure 2.1 23
Figure 2.2 25
Figure 2.3 29
Figure 2.4 31
Figure 2.5 33
Figure 2.6 35
Figure 2.7 37
Figure 2.8 39
Figure 2.9 43
Figure 2.10 45
Figure 3.1 51
Figure 3.2 52
Figure 3.3 54
Figure 3.4 57
Figure 3.5 59
Figure 3.6 60
Figure 3.7 62

Figure 3.8 64
Figure 3.9 66
Figure 3.10 67
Figure 3.11 72
Figure 3.12 74
Figure 3.13 75
Figure 3.14 77

Introduction

The Martian North Polar Layered Deposits (NPLD) are one of the largest water ice reservoirs on the planet, at ~1000 km across and 2 km thick [*Tanaka et al.* 2005]. The NPLD consists of at least 95% pure water ice [*Grima et al.* 2009], but despite this apparently homogeneous composition layering is visible at multiple scales and in multiple data sets [e.g. *Malin and Edgett* 2001, *Fishbaugh and Hvidberg* 2006, *Phillips et al.* 2008]. For years, scientists have believed this layering is connected to global climate cycles, yet efforts to draw a direct correlation between NPLD stratigraphy and the Martian climate have met with mixed success and often produced contradictory results [e.g. *Toon et al.* 1980, *Cutts and Lewis* 1982, *Laskar et al.* 2002, *Milkovich and Head* 2005, *Putzig et al.* 2009].

Studies of high-resolution imagery and topography data have attempted to tie patterns in outcrop layers to orbital cycles [*Laskar et al.* 2002, *Milkovich and Head* 2005, *Perron and Huybers* 2009, *Becerra et al.* 2017]. While some success has been found in correlating outcrop patterns to each other [*Becerra et al.* 2016], establishing a connection between these patterns and the planet's orbital parameters has proven more difficult [*Milkovich and Head* 2008*, Perron and Huybers* 2009, *Becerra et al.* 2017]. Complicating the problem is the fact that the relationship between the surface expression of NPLD layers and their intrinsic properties is difficult to constrain [*Herkenhoff et al.* 2007]. This means that even if scientists were able to definitively connect these layers to a specific climate cycle, it is not clear what that connection would mean.

Thanks to the Shallow Radar (SHARAD) instrument on the Mars Reconnaissance Orbiter (MRO), stratigraphic study of the NPLD is not limited to outcrops. Using SHARAD, scientists have identified dozens of sub-parallel internal reflectors in the NPLD subsurface [*Phillips et al.* 2008]. Radar reflections most often occur at layer boundaries, meaning SHARAD is able to probe the subsurface stratigraphy of the NPLD throughout the entire polar cap. However, studies of radar stratigraphy are not without their own issues. First, it is not clear what types of layers are responsible for radar reflectors in the NPLD. It is commonly believed that layers enriched in dust relative to the surrounding ice are the most likely cause of reflectors [*Nunes and Phillips* 2006, *Phillips et al.* 2008]. The processes responsible for this enrichment remain a topic of debate. Some believe that small fluctuations in ice and dust deposition over time are enough to result in the observed reflectors [*Phillips et al.* 2008, *Putzig et al.* 2009], while others believe that reflectors are caused by thin layers of nearly pure dust left behind as ice sublimates, known as lag deposits [*Levrard et al.* 2007]. This disagreement has led to competing theories for how radar reflectors are tied to global climate change on Mars [*Laskar et al.* 2002, *Levrard et al.* 2007, *Putzig et al.* 2009, *Hvidberg et al.* 2012].

In this dissertation, I attempt to resolve many of the ambiguities presented by radar and outcrop stratigraphy and show that together they can be used to constrain how the ice and dust cycles of Mars have changed over geologic time. In the first chapter, I use a combination of radar reflectivity measurements and modeling to show that previously identified layers known as marker beds could produce reflectors similar to those observed by SHARAD. I also show that previous work has likely underestimated the amount of dust present in these layers, and that there is considerable variability both between and within individual reflectors, implying that local processes are more important than previously thought.

In the second chapter, I show that SHARAD data can be used to infer the composition of individual layers in the NPLD through the use of a refined marker bed model and improved techniques for measuring reflectivity. This is the first time quantitative constraints have been placed on the composition of individual layers in the polar cap. Using this information, I investigate the processes likely responsible for layer formation. I show that while lag deposits are likely not preserved in the NPLD, the small fluctuations in deposition rates predicted by previous work do not account for the amount of dust present in marker beds either. This indicates a significant gap in the scientific community's understanding of how the Martian dust and ice cycles change over orbital time scales.

In the third chapter, I attempt to unify outcrop and radar stratigraphy by making a direct correlation between specific layers visible in an NPLD outcrop and individual SHARAD reflectors. Unfortunately, the limited resolution of SHARAD prevents such a correlation from being achieved, even under ideal conditions. However, I am able to show that radar reflectors and outcrop layers share a similar vertical spacing and both undergo a significant transition at the same elevation, supporting previous hypotheses that the two data sets are responding to the same forcing signal. I also show that if reflectors are indeed caused by marker beds, variations in their reflectivity may be due to small changes in layer thickness, rather than composition. This means that individual SHARAD reflectors could be used to investigate how relative rates of ice and dust deposition have changed both geographically and in time.

This work represents an important step toward unlocking the potential of the NPLD as a global climate record. By integrating multiple techniques and data sets I have shown that local processes are just as important to the formation of the polar cap as larger global trends, and that it is possible to use orbital radar sounding data to place quantitative constraints on how the ice and dust cycles of mars have evolved over orbital time scales.

Chapter 1: New Martian Climate Constraints From Radar Reflectivity Within The North Polar Layered Deposits[1]

1. Introduction:

The North Polar Layered Deposits (NPLD) of Mars are a 2-km-thick formation composed of at least 95% water ice and located in the Planum Boreum region of Mars, roughly centered on the north pole [*Tanaka* 2005, *Grima et al.* 2009]. Despite its apparently homogeneous composition, extensive horizontal layering is visible throughout the ice sheet, both in optical images and in orbital radar sounding data. Cameras such as the High Resolution Imaging Science Experiment (HiRISE) on the Mars Reconnaissance Orbiter (MRO) show visible layering in cliff faces and other outcrops, with layer thicknesses varying between tens of centimeters to almost ten meters [e.g. *Milkovich and Head* 2005, *Herkenhoff et al.* 2007, *Fishbaugh et al.* 2010b], while radargrams from MRO's Shallow Radar (SHARAD) instrument show that the NPLD interior contains discrete packets of sub-parallel horizontal reflectors separated by radar-dark reflector-free zones [*Phillips et al.* 2008].

It has been hypothesized that these layers represent a global climate record of the late Amazonian period, perhaps extending as far back as five million years [*Cutts and Lewis* 1982, *Toon et al.* 1980, *Laskar et al.* 2002, *Tanaka* 2005, *Putzig et al.* 2009]. Orbital eccentricity and obliquity are the main drivers of insolation variability on Mars over long time scales and thus most efforts to explain the NPLD's layering have focused

---

[1] The material presented here is a modified version of previously published work: Lalich, D. E., and J. W.

on these parameters [*Laskar et al.* 2002, *Levrard et al.* 2007, *Putzig et al.* 2009, *Hvidberg et al.* 2012]. However, attempts to correlate orbital forcing to layering as defined by albedo changes, layer morphology, or radar reflectors have resulted in non-unique solutions [*Milkovich and Head* 2005, *Levrard et al.* 2007, *Milkovich et al.* 2008, *Putzig et al.* 2009, *Fishbaugh et al.* 2010b, *Hvidberg et al.* 2012]. Neither radar data nor imagery have proven sufficient to solve this problem individually, but an integration of the two types and disparate scales could yield important advances. An effort to correlate radar reflectors to “marker beds,” erosionally resistant layers visible in cliffs and trough walls, demonstrated that while a direct correlation is challenging, a causal relationship or genetic link is plausible [*Christian et al.* 2013].

Without detailed knowledge of the physical properties of the layers responsible for causing radar reflectors, it is difficult to access the climate information they potentially record. While previous studies have used reflector geometry and stratigraphy in attempts to establish a link between radar reflectors and marker beds, the power of those reflectors has been left largely unexplored. Here, for the first time, we measure and map the reflectivity of three internal NPLD reflectors. We then compare these measured reflectivities to a model approximating marker bed reflectivity, in order to test the hypothesis that SHARAD reflectors are caused by marker beds and to explore how reflectors might be used as a proxy for layer properties. We also compare our results to a climate-driven NPLD accumulation model.

2. Data and Methods

2.1 Radar Data and Study Area

All radar data were acquired by MRO's SHARAD radar sounding instrument. SHARAD uses an 85 μs chirped signal with a 10 MHz bandwidth centered at 20 MHz [*Seu et al.* 2007]. It has a theoretical resolution of 8.4 m in water ice, though in practice this is closer to 10 m [*Seu et al.* 2007, *Nunes et al.* 2011]. It has a cross-track resolution between 3 – 6 km and an along-track resolution of 0.3 – 1.0 km, achieved using synthetic aperture processing techniques [*Seu et al.* 2007]. For this study we used data from a processor developed at NASA's Jet Propulsion Laboratory [*Putzig et al.* 2016]. This differs from the pulse-compressed SHARAD data available in the Planetary Data System in along-track aperture and the ionospheric correction applied, but due to the surface normalization described below, our choice of data processor should not significantly impact the findings.

For this work we chose the "saddle region" of the NPLD as our study area (Fig. 1.1). This region was chosen for its flat and smooth topography, which greatly reduces surface clutter, results in easily identifiable subsurface reflectors, and minimizes surface topographic effects on reflectivity. Three subsurface reflectors were selected based on their ease of identification across multiple radargrams and were mapped throughout the region. All three reflectors are located in the topmost radar reflector packet, which is located within the topmost ~500 m of the deposit [Phillips et al. 2008], reducing the impact of transmission losses and allowing for future comparison to outcrop data.

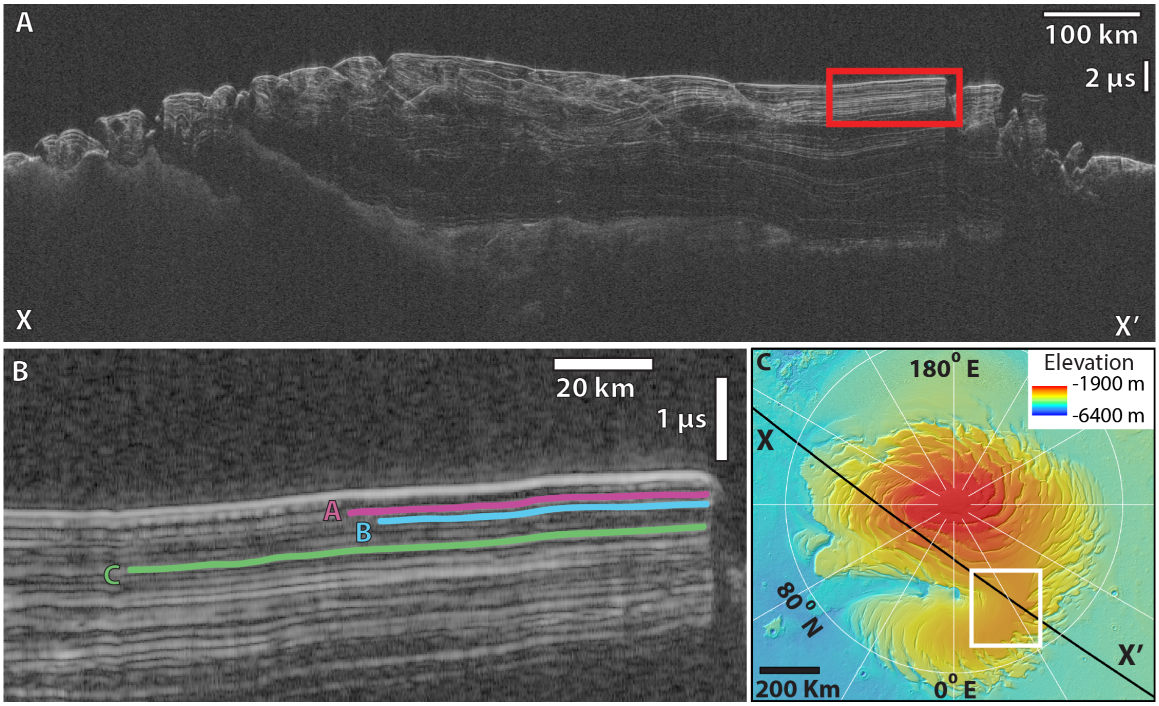

Figure 1.1: A) SHARAD radargram FPA_1716901000, showing the full extent of the NPLD. **B)** Enlarged view of boxed region from A showing the three reflectors mapped for this study. **C)** MOLA colorized elevation context map showing the ground track of the above radargram (black line) and lateral extent of the study area (white box).

2.2 Measuring Reflectivity

To calculate subsurface reflectivity, we used a modified version of the Lauro et al. [2012] model that normalizes to the surface reflection. A schematic outline of this model is shown in Figure 1.2. As surface slopes in this area are typically less than one degree, the model assumes a normal incidence angle for the radar wave. Under this assumption, the power reflected by the surface and subsurface reflector as measured by SHARAD can be expressed as follows:

$$P_s = P_{in} R_s \mathrm{X}_s \tag{1}$$

$$P_{ss} = P_{in}(1 - R_s)^2 R_{ss} \mathrm{X}_{ss} e^{-4\propto d} \tag{2}$$

Where P_s and P_{ss} are the reflected power at the surface and at a given subsurface reflector, respectively. R_s and R_{ss} are the surface and subsurface total power reflectivity, P_{in} is the power incident upon the surface, X_s and X_{ss} are surface and subsurface interface roughness parameters, α is an attenuation parameter with smaller values corresponding to less attenuation, and d is the distance traveled by the wave between the surface and subsurface reflector. When combined and solved for subsurface reflectivity, these equations take the following form:

$$R_{ss} = \frac{P_{ss}}{P_s} \frac{\mathrm{X}_s}{\mathrm{X}_{ss}} \frac{R_s e^{4\propto d}}{(1 - R_s)^2} \tag{3}$$

This equation can be simplified assuming approximately equal surface and subsurface roughness, as well as a low-loss material, which is expected in the NPLD [*Grima et al.* 2009, *Mattei et al.* 2014]:

$$R_{ss} = \frac{P_{ss}}{P_s} \frac{R_s}{(1 - R_s)^2} \tag{4}$$

Thus, the total power reflectivity of a given subsurface reflector is expressed in terms of the power reflected at the surface and subsurface, and the surface reflectivity.

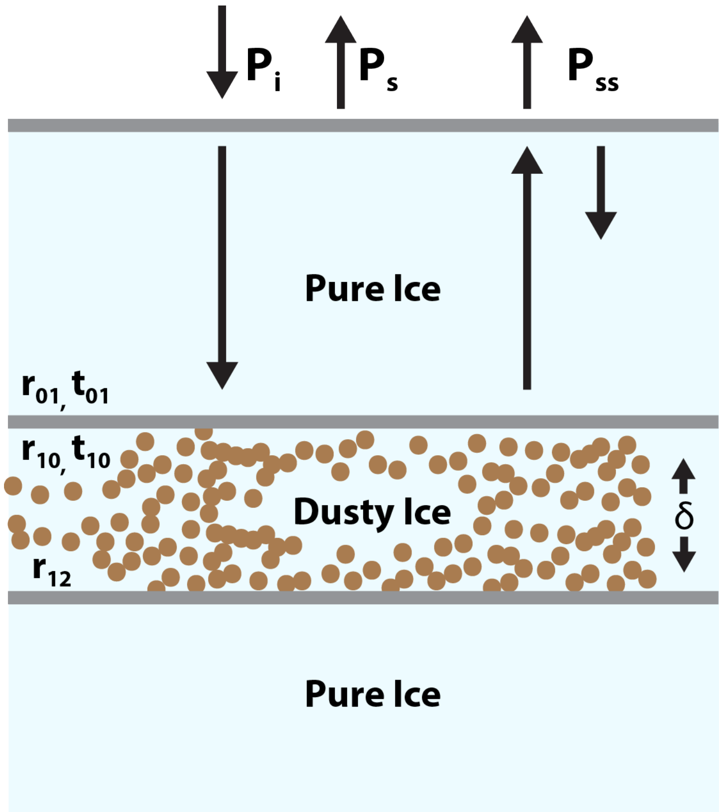

Figure 1.2: Schematic outlining measured quantities and model inputs. Arrows represent traveling radar waves.

Assuming the topmost layer of the NPLD is nearly pure water ice and the permittivity of the Martian atmosphere is approximately equal to that of free space, we can calculate the expected surface reflectivity using the following definition, substituting $\varepsilon_2 = 3.15$ for the dielectric constant of the surface layer:

$$R_s \equiv \left(\frac{1-\sqrt{\varepsilon_2}}{1+\sqrt{\varepsilon_2}}\right)^2 \tag{5}$$

After inserting this assumed surface reflectivity into equation 4, it is possible to estimate subsurface reflectivity using only SHARAD measurements of the power reflected from the surface and subsurface reflector in question.

2.3 Marker Bed Reflectivity Model

The simplest model is to assume that a radar reflection is the result of a single, discrete interface. However, this is likely not the case in the NPLD. It has been suggested that SHARAD reflectors may be related to "marker beds" identified in the NPLD [*Christian et al.* 2013, *Hvidberg et al.* 2012]. Marker beds are erosionally resistant layers distributed at semi-regular intervals throughout the visible NPLD stratigraphy, with thicknesses ranging from 4-8 m [*Malin and Edgett* 2001, *Fishbaugh et al.* 2010a, *Fishbaugh et al.* 2010b]. They are likely enriched in dust or other inclusions relative to their surroundings, making them ideal candidates for the source of radar reflections. However, since their thicknesses are smaller than SHARAD's vertical resolution, they cannot be modeled as simple interfaces. Therefore, we adopt a model used by MacGregor et al. [2011] for estimating the resulting reflectivity of a layer that is thin relative to a given radar wavelength (i.e., two closely-spaced interfaces):

$$R = \left| r_{01} + t_{10} r_{12} t_{01} \left(\frac{e^{-2ik_1\delta}}{1 - r_{12} r_{10} e^{-2ik_1\delta}} \right) \right|^2 \tag{6}$$

Here, r and t are the complex Fresnel amplitude reflection coefficients at each interface, k_1 is the propagation constant in the intermediate layer, and δ is the thickness of that layer. The first subscript of r and t refers to the medium through which the wave is currently travelling, while the second subscript denotes the medium the wave is travelling into. While in principal the materials above and below the thin layer do not have to be the same, here we assume a dust/ice mixture between two layers of pure ice. Because our model does not account for unfilled pore space, modeled dust contents can be thought of as lower bounds. Any additional empty pore space would have to be offset by increased dust content in order to achieve the same reflectivity. Using this model, we can predict the radar reflectivity of a marker bed, given a specific layer thickness and composition, i.e. dust content.

3. Results

3.1 Measured Reflectivities

SHARAD reflectivities in our study area, as determined by Equation 4, are shown in Figure 1.3. Reflectivities are approximately normally distributed between -35 and -3 dB, with the mean reflectivity of each reflector near -18 to -22 dB. This is less than what one would expect from a thin layer of pure generic basalt dust ($\varepsilon = 5.4 - 1 \times 10^{-3}$ i) surrounded by pure ice ($\varepsilon = 3.15 - 6.3 \times 10^{-4}$ i), which would result in a reflectivity of approximately -14.7 dB for a four-meter layer, and only approach observed reflectivities for a narrow range of layer thicknesses. This indicates that marker beds are likely a mixture of both ice and dust, rather than the pure dust lag deposits previously hypothesized [*Toon et al.* 1980, *Levrard et al.* 2007]. One unexpected result is the variation both within and between discrete reflectors. This raises the possibility that local climate conditions are dominating the overall signal in some regions and that they vary over short time and length scales. Local variations are on the order of +/- 15 dB in magnitude, which is approaching the magnitude of the median reflectivity for each mapped reflector (between -17.9 dB and -21.7 dB).

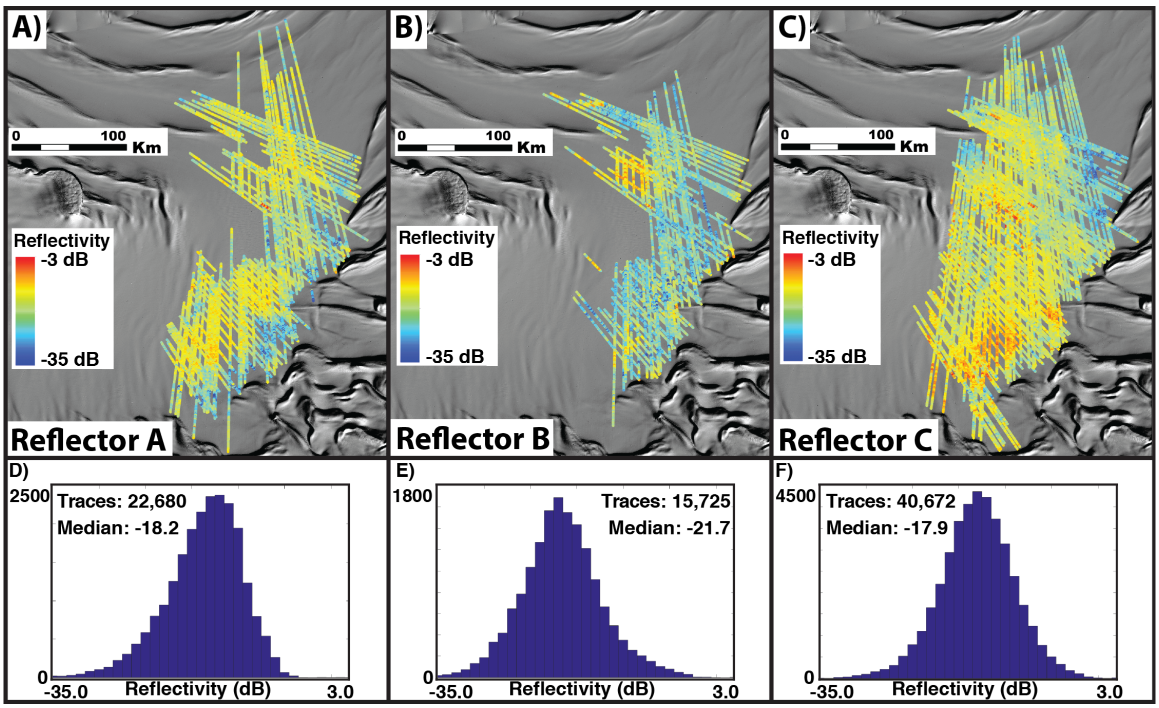

Figure 1.3: **(A-C)** Mapped total power reflectivity for each reflector identified in Figure 1.1. (**D-F)** Histograms of the estimated reflectivity for each reflector with the median value and total number of traces mapped.

3.2 Model Comparison

To compare measured reflectivities to the model, we construct a parameter space of possible reflectivities given known marker bed characteristics. First, using the Maxwell-Garnett mixing formula [*Garnett* 1906], we calculate the complex permittivity for an ice and dust mixture containing a range of dust fractions, with pure ice and pure dust as end members. This range of permittivities is then used to calculate the Fresnel reflection and transmission coefficients to be inserted into Equation 6 along with a range of layer thicknesses between 0.0 and 8.0 meters, creating a parameter space containing the modeled reflectivity for each possible dust percentage-thickness pair. The results of this model are highly dependent on the complex permittivity assumed for the dust. In order to account for a range of plausible dust permittivities, we produce separate models for each of the three dust constituents discussed by Nunes and Phillips [2006], namely ε = 5.4 – 0.001i, ε = 8.8 – 0.017i, and ε = 15.0 – 1.5i which represent a generic basalt, shergottite, and altered basalt, respectively.

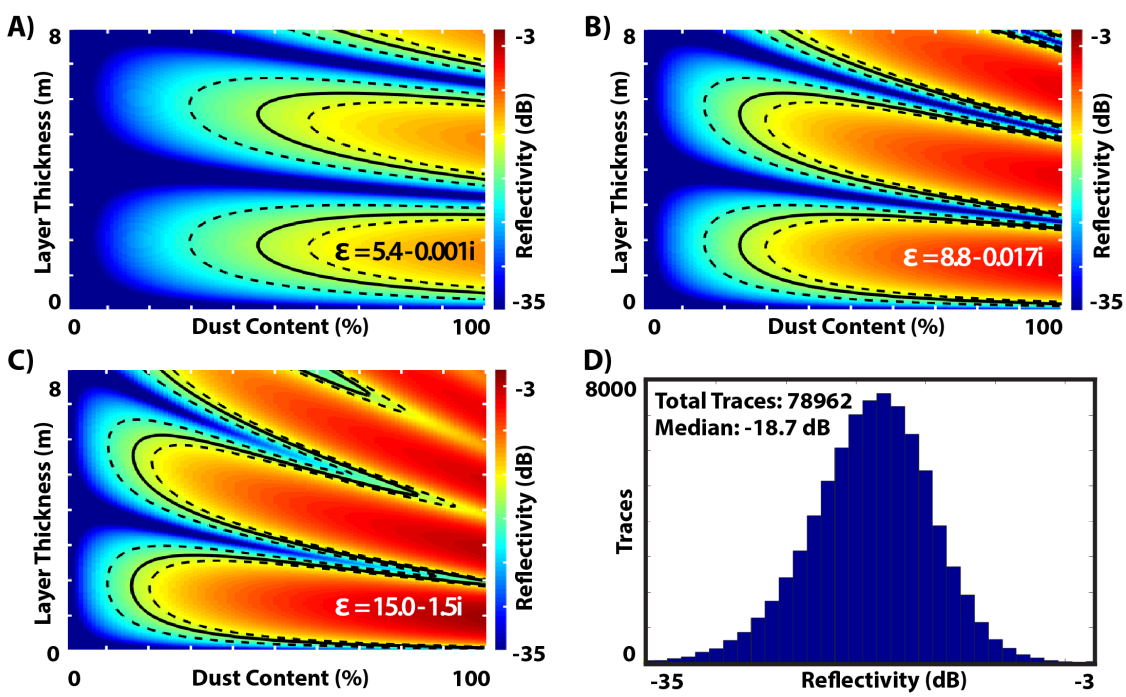

Figure 1.4: (**A-C**) Modeled reflectivities as a function of layer thickness and dust content for each of the three dust constituents discussed in Nunes and Phillips [2006]. Solid black lines are contours of the median measured reflectivity for all three reflectors combined. Dashed lines are contours of the 25th and 75th percentile values for the total distribution of measured reflectivities, shown as a histogram in **D**.

As seen in Figure 1.4, the marker bed model is able to accurately reproduce observed SHARAD reflectivities over a wide range of dust permittivities, layer thicknesses, and compositions. This agreement supports the hypothesis that these relatively thin layers are the source of radar reflections within the NPLD.

4. Discussion

4.1 Reflectors as a Thickness Proxy

This preliminary analysis has great potential when combined with other constraints. As previously mentioned, efforts have been made to correlate SHARAD reflectors with specific marker beds [*Christian et al.* 2013]. A unique correlation might result in constraints on layer thickness or dust content, reducing the model shown here to one dimension and allowing the use of SHARAD reflectivity as a proxy for the remaining unknown variable. We tested this with two scenarios.

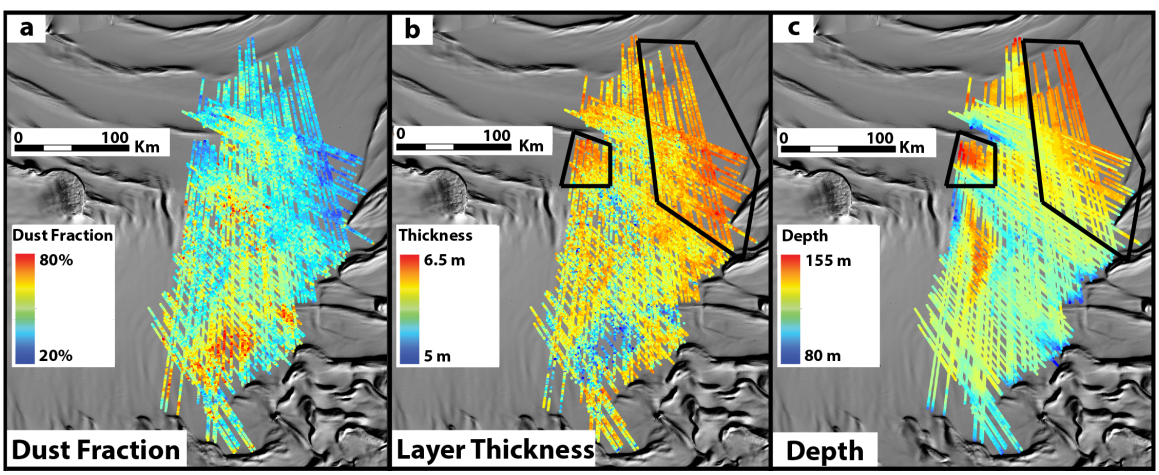

Figure 1.5: **(A)** Map of modeled dust fraction for reflector C assuming constant thickness of 4.0 m and ε_{dust} = 8.8-0.017i. (**B**) Map of modeled layer thickness assuming constant dust fraction of 50% and ε_{dust} = 8.8-0.017i. (**C**) Map of

reflector C depth, assuming a bulk dielectric constant of pure ice for the entire NPLD. Black boxes emphasize correlated areas.

The maps in Figure 1.5A and 1.5B show how either dust content or layer thickness must vary to match reflectivity with the other held constant. The model is far more responsive to changes in layer thickness, requiring just a factor of ~1.5 in thickness change to match observations while a factor of ~4 change in dust content is required if layer thickness is held constant. While only one example is shown in Figures 1.5a and b, other layer thickness/dust fraction values require similar ranges of variation to explain observed reflectivities. Scenarios where dust content is below 10% were not considered, as such scenarios cannot reproduce observed reflectivities. This suggests that while reflectors are caused by the concentration of impurities in marker beds relative to the bulk NPLD composition, it is changes in marker bed thickness, rather than impurity content, which are responsible for geographic reflectivity variation.

If these variations are in fact due to differences in layer thickness, then non-uniform regional ice and dust deposition or ablation is likely the cause. While a single layer represents a relatively short timescale for accumulation, we can test this for longer timescales by examining the depth to these reflectors from the surface. As shown in Figure 1.5B and 1.5C, there is a qualitative correlation between the measured reflectivity (as represented by layer thickness) and reflector depth from the surface, particularly in some regions as indicated by boxes in the figures. Similar correlations exist for each mapped reflector, supporting the hypothesis that changes in reflectivity are due to variations in layer thickness rather than composition. These correlations are unlikely to be caused by the previously neglected attenuation losses; in two of our three mapped reflectors deeper regions are brighter than their shallower surroundings.

However, there are some patterns in reflectivity that are not evident in reflector depth. This suggests that either other processes are involved in determining reflectivity, or that some regional deposition patterns change on short enough time scales to vary between layers. Some variation is also likely due to changes in surface reflectivity since our calculations normalize to the surface return. As explained in section 2.2 we have assumed a constant surface reflectivity, but Grima et al. [2012] did find variations in surface reflectivity. Accounting for this would likely "smooth out" some of the observed reflectivity anomalies, but given the magnitude of variations observed by Grima et al. [2012] this cannot account for the full range of reflectivity that we observe, nor the geographic variability

The modeled geographic variation in marker bed thickness shown in Figure 1.5B falls within the range reported by Becerra et al. [2016], which was obtained through analysis of marker bed sequences in multiple HiRISE digital elevation models (DEMs). One limitation of such image-based analysis is that it can only be performed at outcrops, such as trough walls. After analyzing 16 sites, Becerra et al. [2016] could only confidently apply their results to the upper 500 m of 7% of the NPLD. SHARAD is not as limited; reflectors can be accurately traced across the majority of the NPLD. Using DEM analysis to constrain the model presented here could allow for the complete reconstruction of the accumulation history of the NPLD.

4.2 Climate Model Comparison

Recent work by Smith et al. [2016] correlated reflector C to a Mars obliquity shift that occurred ~400,000 years ago, providing an age constraint. This age constraint allows us to directly compare our mapped reflectors to a model of NPLD accumulation [Hvidberg et al. 2012]. This model uses insolation to drive changes in the deposition rates of ice and dust, estimating the stratigraphy and composition of layers similar to marker beds. As shown in Figure 1.6, the model-predicted layers strongly resemble the observed SHARAD reflectors under the assumption that reflector C is approximately 400,000 years old. This suggests that the climate-driven deposition model is approximately reproducing the formation time of marker beds, and that these marker beds are responsible for SHARAD reflectors.

However, the accumulation model predicts dust content to be no more than ~5% for all but a handful of layers. As shown in Figure 1.4, this is not enough dust to cause the bright SHARAD reflectors observed in the NPLD. At the accumulation model's peak dust deposition rate of ~0.02 mm/year, the ice deposition rate would have to drop to ~0.13 mm/year to reach 15% dust, the lowest possible impurity value that still results in reflectivities near observations. Such a low ice deposition rate is inconsistent with average deposition rates near ~0.8 mm/y [*Smith et al.* 2016] and the fact that many of these layers are predicted to form during periods of peak ice deposition [*Hvidberg et al.* 2012]. This implies that these lower ice deposition rates are not feasible, and therefore our inferred dust content values cannot be met without increasing the dust deposition rate at the NPLD, at least over short timescales.

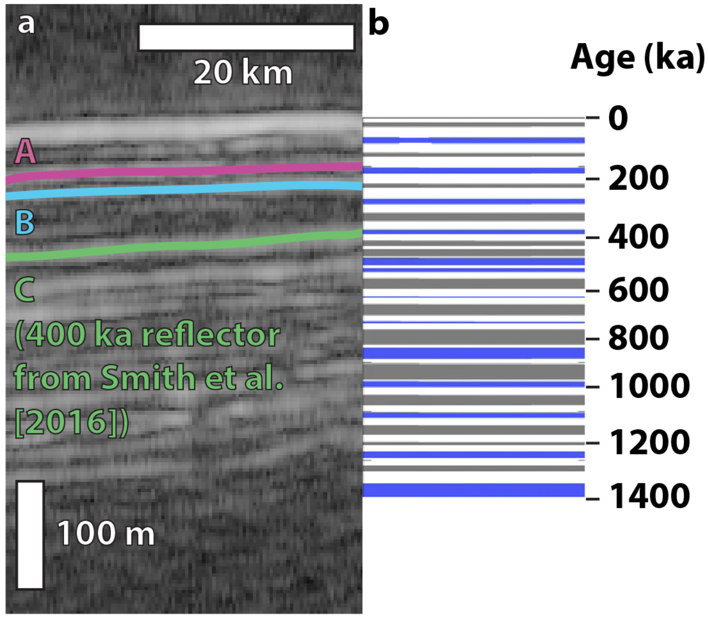

Figure 1.6: A) Section of the radargram shown in Figure 1.1b with the mapped reflectors traced and labeled in color. **B)** Section of the NPLD deposition model reproduced from Figure 10(D) of Hvidberg et al. [2012] and stretched so that the surface and ~400 ka layer match the radargram with age constraint from Smith et al. [2016]. Blue layers are formed during periods of low ice deposition, while grey layers are formed during periods of high dust deposition.

5. Conclusions

Our work can tie measured marker bed thicknesses, radar reflectivities, and climate models together into a self-consistent picture for the first time. Variations in bed thickness, dust content, or some combination of the two can explain the observed geographic variability of reflectivity, although comparisons with reflector depth and outcrop stratigraphy indicate that layer thickness variation is the most likely cause. This implies that SHARAD reflectors can be used as a proxy for relative accumulation rates both spatially and temporally within the NPLD. Additional physical constraints are required in order to determine this uniquely. Comparison to an NPLD accumulation model shows that previous attempts to reconstruct the NPLD may be underestimating the deposition rate of dust at the NPLD in the past ~400,000 years. In lieu of a positive, direct correlation of radar reflectors with visible outcrops that might provide a constraint on layer thicknesses at a discrete point, a future radar sounder with ~10x higher vertical resolution would be required to discriminate between the different possibilities in our model.

Chapter 2: Icy Dust or Dusty Ice? Using Radar Reflectivity as a Proxy for the Dust Content of Individual Layers in the Martian North Polar Layered Deposits

1. Introduction

The North Polar Layered Deposits (NPLD) of Mars represent one of the largest reservoirs of water ice on the planet, covering a quasi-circular region 1000 km in diameter and ranging in thickness between 1.5 and 2.0 km [*Tanaka* 2005]. Thousands of sub-parallel layers are visible in both optical imagery, giving the formation its name, and radar sounding data reveals dozens of reflectors with similar geometry [*Christian et al.* 2013]. Analogous to layering in polar ice on Earth, the NPLD are thought to record information on Mars' climate [e.g. *Toon et al.* 1980, *Cutts and Lewis* 1982, *Laskar et al.* 2002]. The NPLD is thought to be roughly four million years old [*Levrard et al.* 2007, *Greve et al.* 2010], yet evidence suggests the uppermost surface is extremely young and possibly in net positive accumulation in the present day [*Herkenhoff and Plaut* 2002, *Tanaka* 2005, *Brown et al.* 2015, *Landis et al.* 2016]. Because NPLD accumulation is affected by climate, the polar cap may record valuable information about how the Martian climate has evolved in the recent past. However, efforts to link layering or reflector properties to climate processes have produced mixed results. Stratigraphic sections visible in outcrops have been shown to contain cyclic bedding features [*Milkovich and Head* 2005, *Milkovich et al.* 2008, *Perron and Huybers* 2009, *Hvidberg et al.* 2012, *Becerra et al.* 2017], but the period and scale of these features is non-uniform across the cap and connecting them to climate conditions remains a challenge [*Hvidberg* *et al.* 2012, *Becerra et al.* 2016]. Some success has also been found in correlating Mars' modeled orbital dynamics [*Laskar et al.* 2002, *Levrard et al.* 2007] to large packets of radar reflectors [*Phillips et al.* 2008, *Putzig et al.* 2009, *Hvidberg et al.* 2012] and an unconformity in the upper section of the NPLD [*Smith et al.* 2016]. However, these correlations are often inconsistent, and are too broad to enable the use of radar reflectors as a detailed climate record. Recent work has suggested that these radar reflectors may share a genetic link with the outcrop stratigraphy, and indeed some research has pointed to specific layers known as "marker beds" as a plausible source for radar reflectors [*Christian et al.* 2013, *Lalich and Holt* 2016].

In an effort to fill these knowledge gaps and clarify the relationship between NPLD layering and the Martian climate, we have constructed radar reflectivity profiles of sites across the NPLD. Combining these measured reflectivities with a thin layer reflection model based on the one presented in *Lalich and Holt* [2016] allows us to infer the relative dust content of individual layers. This observed dust content is then compared to the concentration predicted by a previously published model of NPLD accumulation, which used Mars' orbital parameters to predict how the deposition rates of ice and dust varied in the relatively recent past at the planet's north pole [*Hvidberg et al.* 2012].

2. Background

2.1 Outcrop Stratigraphy

Malin and Edgett [2001] were the first to define the original "marker bed," and identify it in multiple images across different outcrops. Soon after, others were able to more definitively correlate sequences containing this original marker bed and others like it throughout the NPLD [*Fishbaugh and Hvidberg* 2006, *Fishbaugh et al.* 2010b, *Becerra et al.* 2016]. *Laskar et al.* [2002] and *Milkovich and Head* [2005] found that these sequences contained a periodic signal, with a peak spectral wavelength of ~20-30 m. This periodic behavior was interpreted as the result of differences in ice and dust accumulation at the north pole due to Mars' insolation cycle. *Perron and Huybers* [2009] failed to detect this same behavior at a statistically significant level, but were able to identify a signal at ~1.6 m spatial wavelength.

Later work showed that albedo profiles are prone to obfuscation by surface processes or imaging conditions [*Herkenhoff et al.* 2007, *Fishbaugh et al.* 2010a]. Instead, high-resolution topography was suggested as a supplemental means of dividing layers based on intrinsic physical properties [*Fishbaugh et al.* 2010a]. *Becerra et al.* [2016] showed that sequences of ablation-resistant layers identified using high-resolution digital terrain models (DTMs) in combination with imagery are indeed more easily correlated with each other across the NPLD than brightness profiles alone. Further investigation showed that these sequences might contain dominant periodicities with similar ratios to those found in the modeled insolation record [*Becerra et al.* 2017]. This connection remains tenuous, however, as errors in periodicity measurements are large and identification of signals is inconsistent from outcrop to outcrop. Furthermore, while identifying such a connection between visible layering and insolation cycles represents an important step forward, it is difficult to use these techniques to constrain individual layer properties.

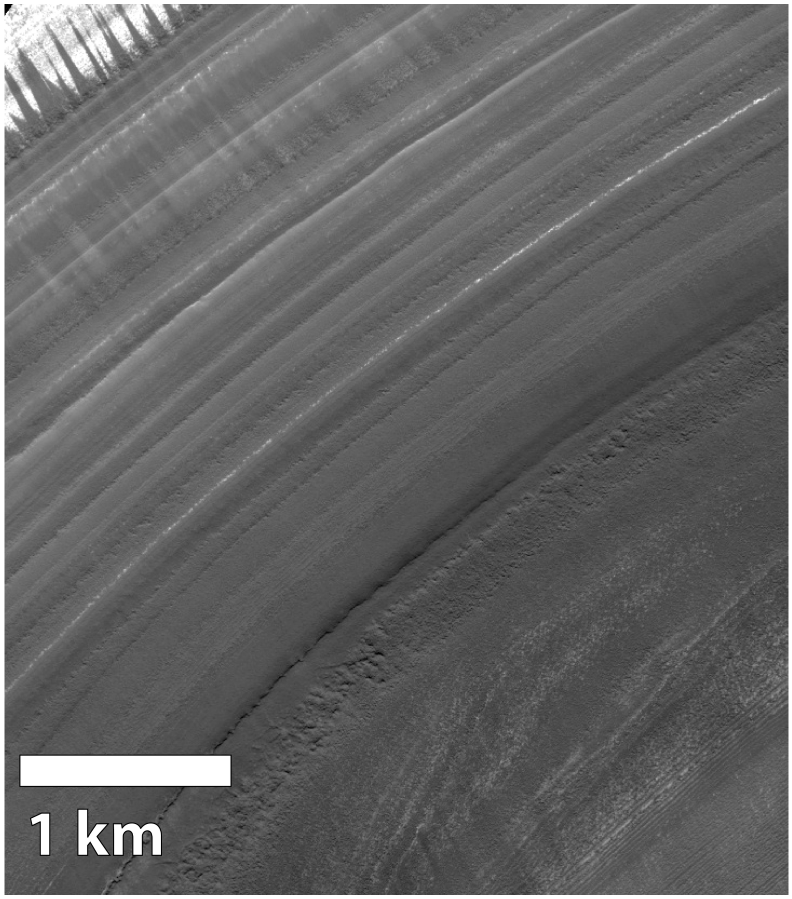

Figure 2.1: Portion of HiRISE image ESP_018870_2625 showing a typical layer sequence at a trough wall. The outcrop slopes to the bottom right of the image.

2.2 Radar Stratigraphy

In addition to the work done with outcrop stratigraphy, many have attempted to tie radar reflectors visible in data collected by the Shallow Radar (SHARAD) orbital radar sounder to the Martian paleoclimate. In general, radar reflections are caused by abrupt changes in subsurface permittivity. These changes typically occur at the boundaries between layers made up of different materials. In the NPLD, it is believed that reflections are the result of layers of ice enriched in dust relative to the material around them [*Nunes and Phillips* 2006]. This enrichment is likely the result of some change in the accumulation rate of dust or ice, reflecting the climatic conditions at the time of deposition. Several forcing scenarios have been proposed [*Philips et al.* 2008, *Putzig et al.* 2009, *Hvidberg et al.* 2012], but the exact mechanism remains unclear.

Phillips et al. [2008] identified four discrete packets of reflectors in the NPLD separated by radar-dark interpacket regions of presumably more pure ice. They interpreted this large-scale structure as the result of cyclic changes in ice and dust accumulation due to variations in Mars' eccentricity and obliquity. Further work by *Putzig et al.* [2009] modified this interpretation by correlating reflector packets to low amplitude variations in the insolation function, rather than obliquity, and presented the hypothesis that reflector-causing layers are formed by fluctuations in dust content during periods of relatively constant ice deposition. This interpretation is contradictory toward previous work by *Levrard et al.* [2007], which hypothesized the formation of layers through sublimation lag deposits during periods of high amplitude insolation oscillations. This ambiguity has yet to be resolved.

More recent work has attempted to establish correlations between imagery-based outcrop stratigraphy and radar stratigraphy. *Christian et al.* [2013] applied signal analysis techniques to radar traces near a trough wall and found that while some peak wavelengths were shared between the radar data and the nearby stratigraphic profile, many were not. Still, this suggests some common forcing mechanisms between the two stratigraphies. *Lalich and Holt* [2016] compared reflectivities of three mapped SHARAD reflectors to those predicted by a model approximating marker bed reflection, and while they found that the model was capable of accurately reproducing the observations, they were unable to place tight constraints on layer properties. They also found that radar reflectivity varies greatly both within and between reflectors. They attributed both forms of variation primarily to differences in layer thickness, proposing that radar reflectivity could potentially be used as a proxy for relative deposition rates. Despite these advances, the connection between radar reflectors and marker beds remains somewhat tenuous.

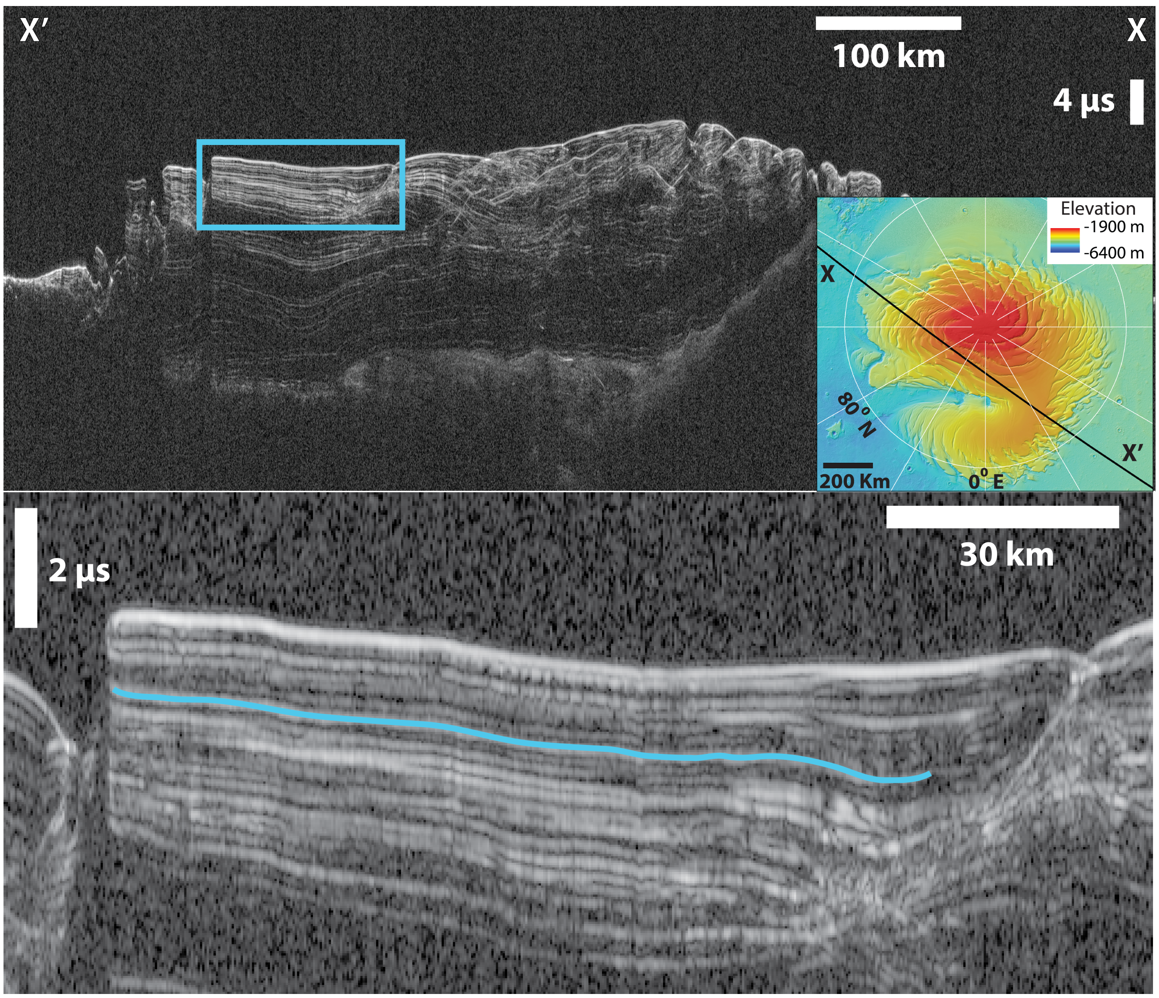

Figure 2.2: Top) SHARAD radargram 1716901000 crossing the NPLD. Blue box shows the location of expanded section. Inset is a MOLA colorized elevation map of the NPLD containing the radargram ground track. **Bottom)** Enlarged portion of the full radargram showing the top reflector packet in detail. The reflector traced in blue is the cap-wide reflector discussed in the text.

2.3 Layer Formation Processes and Climate Modeling

In general, the composition of NPLD layers is determined by changes in the relative rates of dust and ice accumulation. As previously discussed, two processes have been proposed that could potentially form layers with high enough dielectric contrasts to cause radar reflections [*Lalich and Holt* 2016]. The first process involves the accumulation and subsequent sublimation of ice from a dusty ice layer. Any dust impurities present in the layer will be left behind when the ice sublimates, forming a more pure dust layer on the surface, with relatively low interstitial ice content. Once enough dust builds up on the surface, it acts as an insulator, preserving the ice underneath [*Toon et al.* 1980, *Levrard et al.* 2007]. Exactly how much dust is required to create such a deposit is a matter of debate, but estimates place the layer thickness necessary to fully insulate the underlying ice between a few millimeters and roughly one meter [*Hofstadter and Murray* 1990, *Skorov et al.* 2001]. The second suggested process for creating polar layers involves smaller fluctuations in the relative deposition rates of ice and dust. Rather than forming during periods of ice removal, in this scenario reflector-causing layers are constructional features, formed when climate conditions facilitate significant deviation in average deposition rates [*Cutts and Lewis* 1982, *Laskar et al.* 2002]. These layer formation processes are not necessarily mutually exclusive, but they are expected to be active during opposite periods in the planet's orbital cycle [*Hvidberg et al.* 2012], and if both are indeed responsible for reflector-causing NPLD layers then it becomes difficult to explain the interpacket regions present within the cap.

Hvidberg et al. [2012] modeled NPLD accumulation using ice and dust deposition rates forced by the planetary obliquity cycle. Their model allowed for creation of layers using both processes discussed above. Rather than dividing layers into lag deposits and constructional layers, they instead observed a dichotomy between layers formed during periods of high dust deposition, and those formed during periods of low ice deposition, of which lag deposits are a subset. Broadly speaking, the model predicted these layering processes to occur 180 degrees out of phase in the obliquity cycle, resulting in an alternating pattern of "high dust deposition" and "low ice deposition" layers. These two types of layer-forming mechanisms produced distinct ranges of dust contents. Layers formed during peak dust deposition periods typically had less than 5% dust content, while those formed during periods of minimum ice deposition often had dust contents above 5%. These high dust content layers were often found in packets, similar to the stratigraphic structure seen in radar data. This finding suggested that radar reflectors are the result of layers formed when ice accumulation is lowest, and in some cases possibly by lag deposits.

3. Data and Methods

3.1 SHARAD data and study sites

The shallow radar instrument (SHARAD) is an orbital radar sounder on the Mars Reconnaissance Orbiter. It uses a chirped signal with a bandwidth of 10 MHz at a 20 MHz center frequency transmitted in an 85 us pulse [*Seu et al.* 2007]. SHARAD's nominal range resolution is 8.4 m in water ice, though in practice this can approach 20 m in the NPLD due to non-ideal imaging conditions and interference with nearby reflectors [*Seu et al.* 2007, *Nunes et al.* 2011]. Cross-track resolution is between 3-6 km, while an along-track resolution of 0.3-1 km is achieved using synthetic aperture processing [*Seu et al.* 2007].

In order to select sites for the extraction of radar profiles, a previously mapped cap-wide radar reflector associated with a proposed climatic change [*Smith et al.* 2016] was used as context (Figs. 1 and 3). Ten sites with widely varying local reflectivities were chosen to expand upon a previous study that showed regional horizontal variability of SHARAD data [*Lalich and Holt* 2016]. Many of the new sites were chosen in regions of the NPLD that are difficult to link directly to the other sites using traditional means, due to the disconnection of layering across troughs. Methods to connect these discontinuous sections are described in *Smith and Holt* [2015]. The three remaining sites were chosen in the "saddle region" of the NPLD, similar to our previous study [*Lalich and Holt* 2016], which connects the main lobe of the polar cap to the Gemina Lingula formation. These three sites are linked via continuous subsurface reflectors, confirming that any profiles extracted from these sites will sample the same subsurface layer sequence. All sites were also chosen with a preference for dense radar coverage.

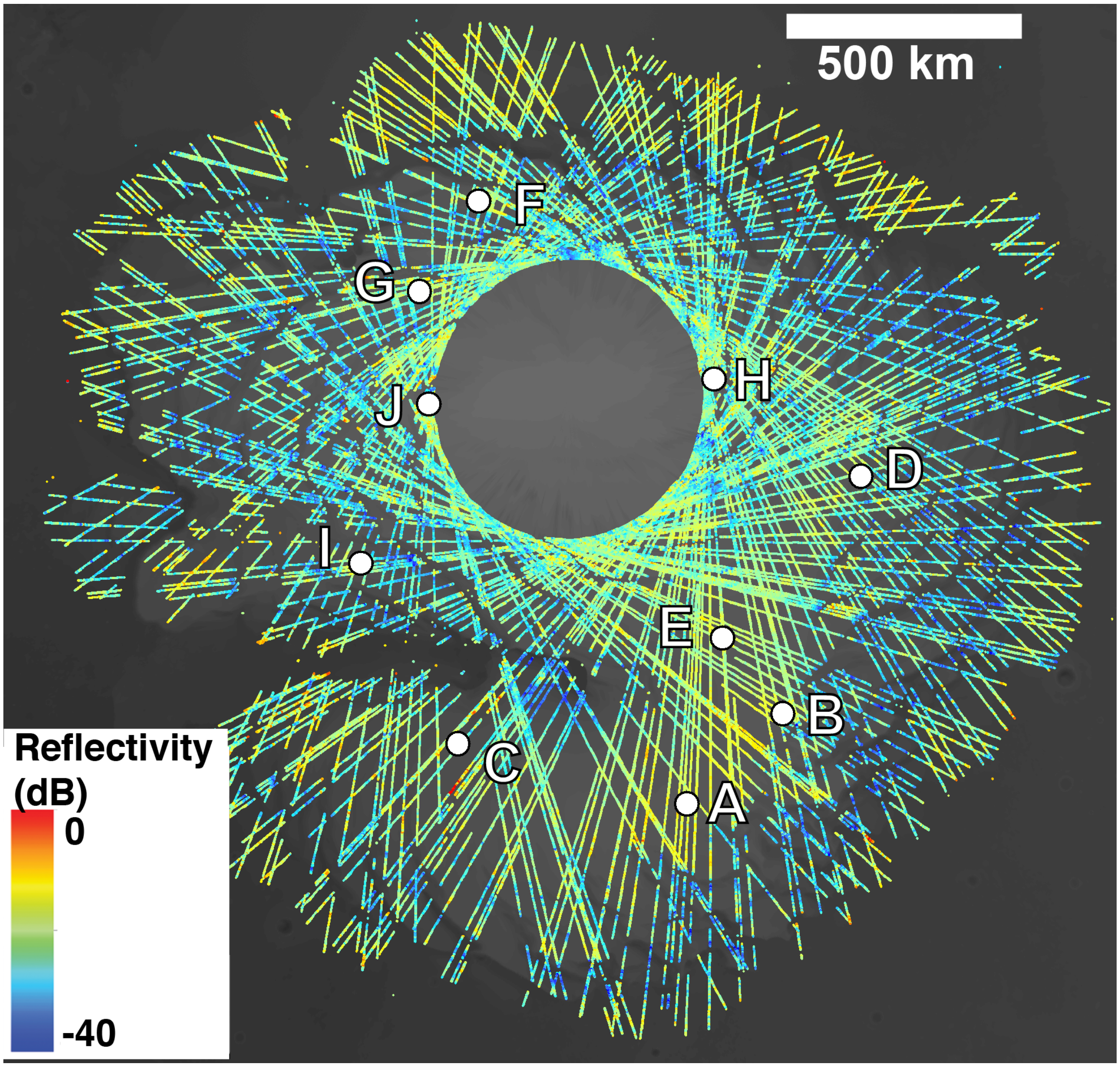

Figure 2.3: Map of the cap-wide reflector used as context for this study. White dots denote sites for which radar profiles were created. Color corresponds to reflectivity measured using the technique described in sections 3.2.

3.2 Measuring Radar Reflectivity

In order to facilitate comparisons of radar reflectivity with modeled paleoclimate conditions, profiles of radar reflection power vs. depth were constructed at each study site. All radar traces within one Fresnel zone (3 km) of a central latitude and longitude were selected and averaged together to form a representative radar profile. Before averaging, traces at each site were shifted to align their first returns, and thus reduce any depth differences introduced by local surface slopes or relative shifts due to varying ionospheric delays. The number of traces selected at each site varied between 16 and 107, with sites closer to the pole generally including a larger number of traces due to more dense radar coverage.

Once profiles were constructed, reflectors within 500 m of the surface (assuming a dielectric constant equivalent to water ice [*Grima et al.* 2009]) were automatically chosen by selecting every point in the reflection power vs. depth record that corresponded to a local maximum. This depth limit was chosen to constrain our analysis to the first reflector packet, enabling direct comparisons to previously mapped outcrop stratigraphy and limiting the effect of propagation losses. Depth values were calculated from the radar time delay assuming a wave velocity below the surface consistent with propagation in pure ice ($\varepsilon = 3.15$). In order to avoid erroneously identifying peaks in the background noise as reflectors, only maxima with reflection powers above -35 dB were considered. This lower bound ensures that no background noise is mistakenly included in reflectivity estimates, but also introduces the possibility that some low-power reflectors were overlooked, given that it is slightly higher than SHARAD's nominal noise floor of -40 dB. Such dim reflectors are likely rare within the first 500 m of the SHARAD record, given the low-loss nature of the NPLD [*Grima et al.* 2009] and the range of reflector powers previously observed [*Lalich and Holt* 2016].

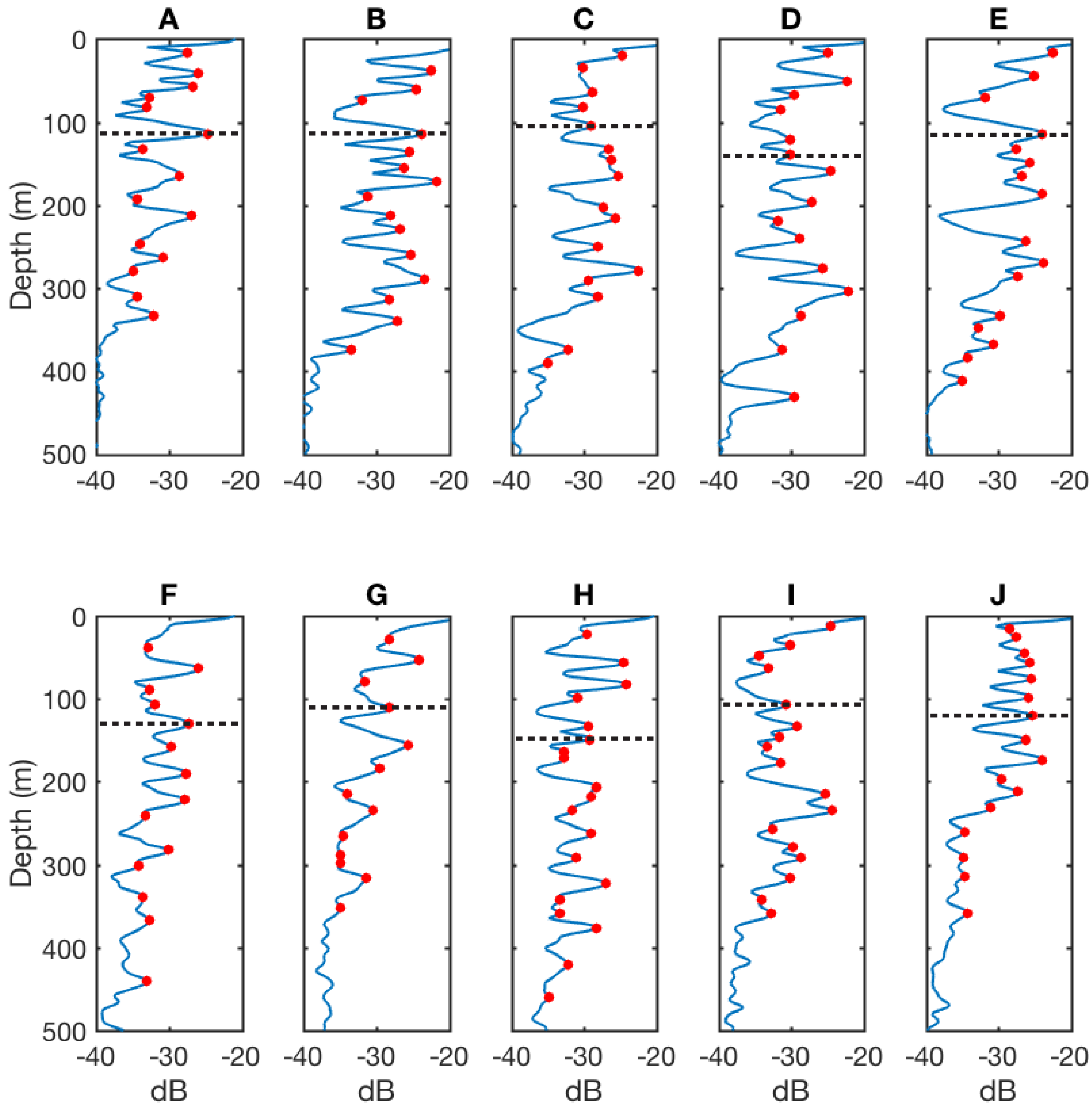

Figure 2.4: Average reflection power profiles extracted at each site. Red dots correspond to local maxima selected as reflectors. Dotted lines mark the cap-wide reflector discussed in the text and shown in Figure 3.

These subsurface reflector powers are then used to calculate the total power reflectivity for each subsurface interface. This was done using a method based on that of *Lalich and Holt* [2016] for the upper reflector packet, which was itself adapted from

Lauro et al. [2012]. In this approach, subsurface reflectivity (R_{ss}) is expressed as a function of observed reflection power at the surface and subsurface (Respectively, P_s and P_{ss}), the surface reflectivity (R_s), and an estimate of power lost due to propagation in the medium. Our approach differs from that of previous work in two significant ways. First, instead of using a constant value for R_s derived from the assumed composition of the surface layer, we use observationally determined values from *Grima et al.* [2012], selecting the reflectivity value from the location closest to each individual radar profile. This allows us to further reduce the influence of non-uniform surface properties on the calculation of subsurface reflectivity. The second significant change is the adoption of an observationally based NPLD loss tangent of $\tan\delta = 0.0026$ [*Grima et al.* 2009] in order to express transmission losses, rather than using a theoretical value [*Lauro et al.* 2012] or simply assuming negligible losses [*Lalich and Holt* 2016]. Given the low value of the loss tangent, we adopt the approximation $\tan\delta \approx \delta$. These alterations result in the following expression to determine subsurface reflectivity:

$$R_{ss} = \frac{P_{ss}}{P_s} \frac{R_s e^{2\delta kz}}{(1-R_s)^2} \tag{1}$$

Where k is the wavenumber and z is the depth below the surface. Reflectivity estimates were made for every identified reflector.

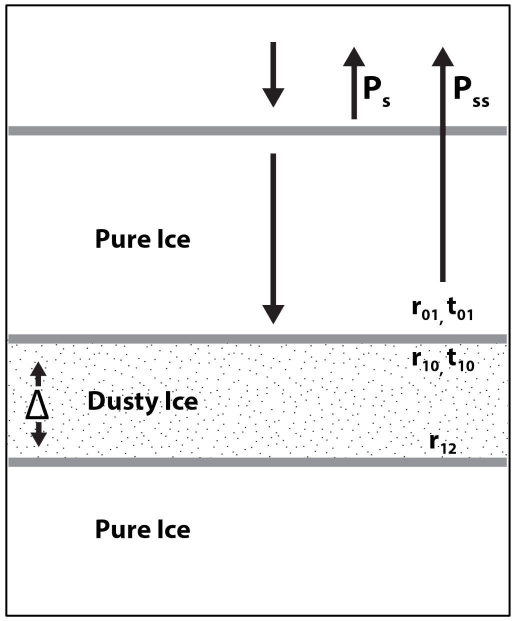

Figure 2.5: Schematic showing the various measured and modeled parameters discussed in section 3.

3.2 Modeling Marker Bed Reflectivity and Estimating Dust Content

Marker beds are typically thinner than SHARAD's range resolution, meaning they cannot be modeled as a simple interface. Instead, we apply the technique developed by *MacGregor et al.* [2011] to model the effective reflectivity of two interfaces that are closely spaced relative to radar wavelengths, i.e. a thin layer. This model was previously used to simulate marker bed reflectivity by *Lalich and Holt* [2016], and can be expressed as follows:

$$R = \left| r_{01} + t_{10} r_{12} t_{01} \left(\frac{e^{-2i\gamma\Delta}}{1 - r_{12} r_{10} e^{-2i\gamma\Delta}} \right) \right|^2 \quad (2)$$

Where reflectivity (R) is expressed in terms of the Fresnel reflection and transmission coefficients at each interface (r_{xx} and t_{xx} where the first subscript is the layer through which the wave is propagating and the second is the layer it is incident upon), the complex propagation constant in the thin layer (γ), and the thickness of that layer (Δ). In order to calculate the Fresnel reflection and transmission coefficients, we first assume the thin layer is composed of a dust and ice mixture and is bounded above and below by pure water ice. Then, we calculate a range of permittivities for this mixture using the Maxwell-Garnett mixing formula [*Garnett* 1906], with pure ice and pure dust as end members. This necessitates selecting a permittivity value for the dust inclusions. *Nunes and Phillips* [2006] proposed three potential values for Martian dust permittivity. We selected the intermediate value ($\varepsilon = 8.8 - 0.017i$) for this work, which is the value corresponding to a shergottite. Using this range of mixture permittivities, we are able to calculate the reflection and transmission coefficients necessary for the model input for each dust content value. In order to construct the full parameter space of possible marker bed configurations, we consider a range of thicknesses between one and ten meters. We then use equation 2 to calculate the reflectivity for each dust content-thickness pair.

In contrast to *Lalich and Holt* [2016], who limited the model to SHARAD's center frequency, here we include the full bandwidth of the transmitted chirp signal. By repeating the procedure outlined above for every frequency sampled by the SHARAD chirp, we can build a three dimensional parameter space of reflectivity as a function of dust content, layer thickness, and frequency. As SHARAD is limited to a finite bandwidth, the Fourier transform of the transmitted chirp can be interpreted as an energy density function, describing how much power is transmitted at each frequency. While the spectral properties of the transmitted signal are weakly dependent on the temperature of the radar transmitter and receiver, differences are minor and do not affect the overall shape of the energy distribution. For this study, we use the SHARAD reference chirp corresponding to transmitter and receiver temperatures of 0° C, obtained from NASA's Planetary Data System.

Multiplying our parameter space across the frequency axis by this density function and then integrating over all frequencies allows us to express the total reflectivity as observed by SHARAD as a function of only dust content and layer thickness, while accounting for the non-uniform distribution of energy across the frequency bandwidth.

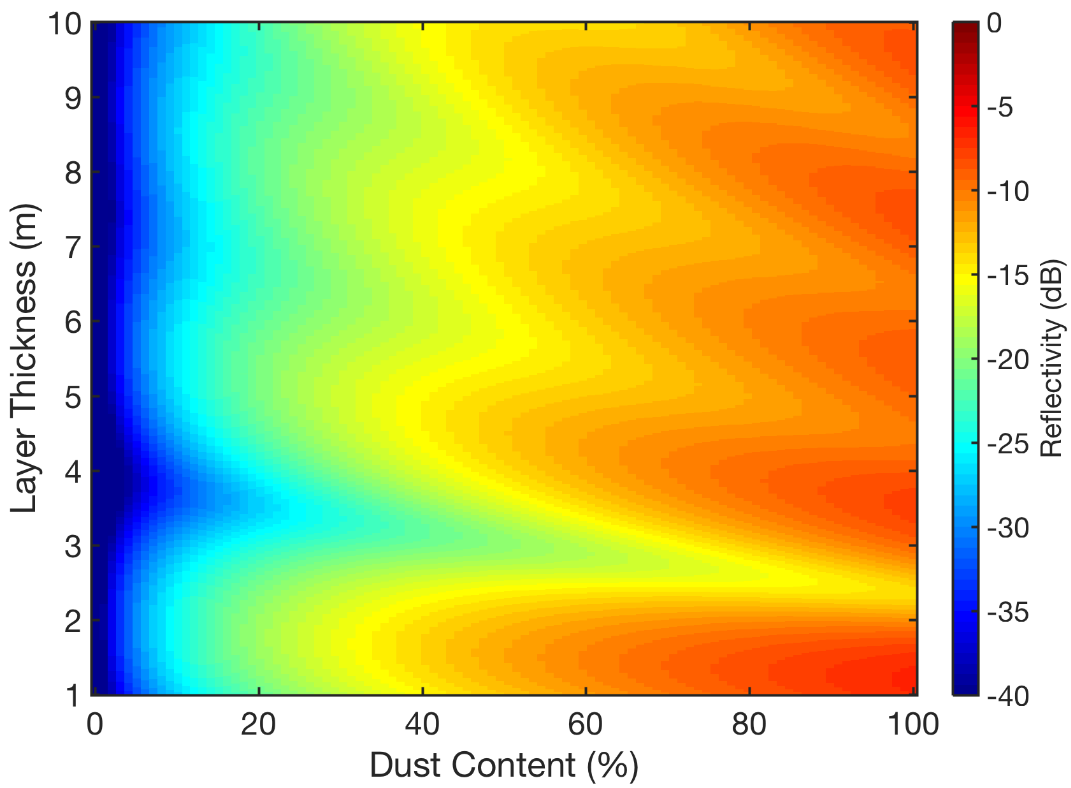

Figure 2.6: Modeled marker bed reflectivity for bed thicknesses between 1-10m and fractional dust contents between 1-100%.

This new model differs significantly from those shown by *Lalich and Holt* [2016] and allows for more direct comparisons with radar observations. Notably, contours of constant reflectivity are limited to narrow ranges of dust content, even as the layer thickness varies by an order of magnitude. This means that by measuring SHARAD reflectivity as outlined above it is possible to place constraints on the fractional dust content of individual layers. For every layer thickness value, we record the dust content needed for the modeled reflectivity to match a given observed reflectivity. Assuming all modeled layer thicknesses are equally probable, this allows us to construct a distribution of possible dust content values for each analyzed reflector. An example of this procedure is shown in Figure 7.

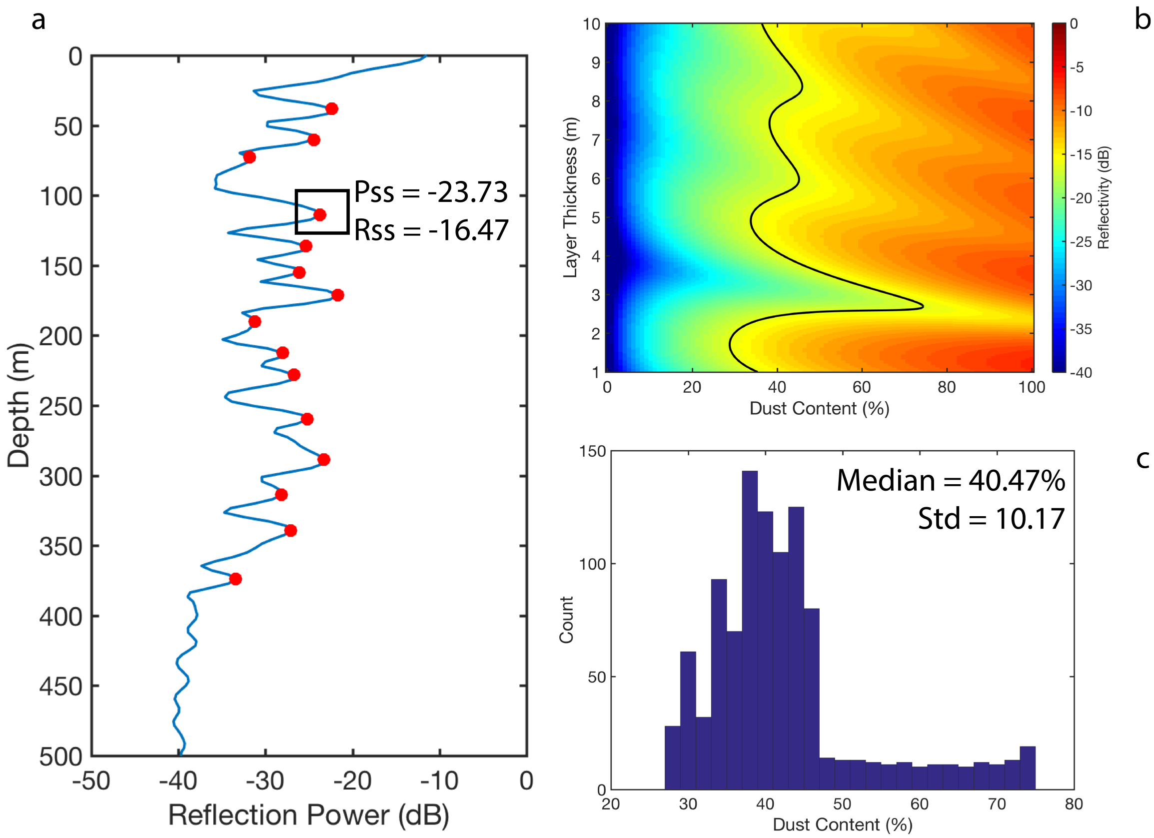

Figure 2.7: Outline of process for estimating dust content. **a)** Reflection power vs. depth for site B. Black box shows which reflector is used for b) and c). Annotations show values for this reflector's measured reflection power (Pss) and reflectivity (Rss). **b)** The model described in section 3.2, with a contour of constant reflectivity at the value shown in a), or -16.47 dB. **c)** The distribution of all dust content values for the contour shown in b), along with the median and standard deviation. Note the long tail caused by layer thicknesses between ~2 and 4 m.

4. Results and Discussion

4.1 Reflectivity as a Dust Proxy

When the above procedure is applied to the study sites discussed in section 3.1 we retrieve a wide range of possible dust contents. The inferred dust content for each reflector at all five sites can be found in the supplementary material. There were between 13 and 19 reflectors identified at each site within the top 500 m of the NPLD. Plots of the median inferred dust content for each reflector at each site as a function of depth are shown in Figure 8. Histograms of these data are shown in Figure 9. These results show that reflectors can vary between ~10% – 60% dust within a single site, implying drastic differences in climate conditions through time, even during periods that result in similar types of stratigraphic layers.

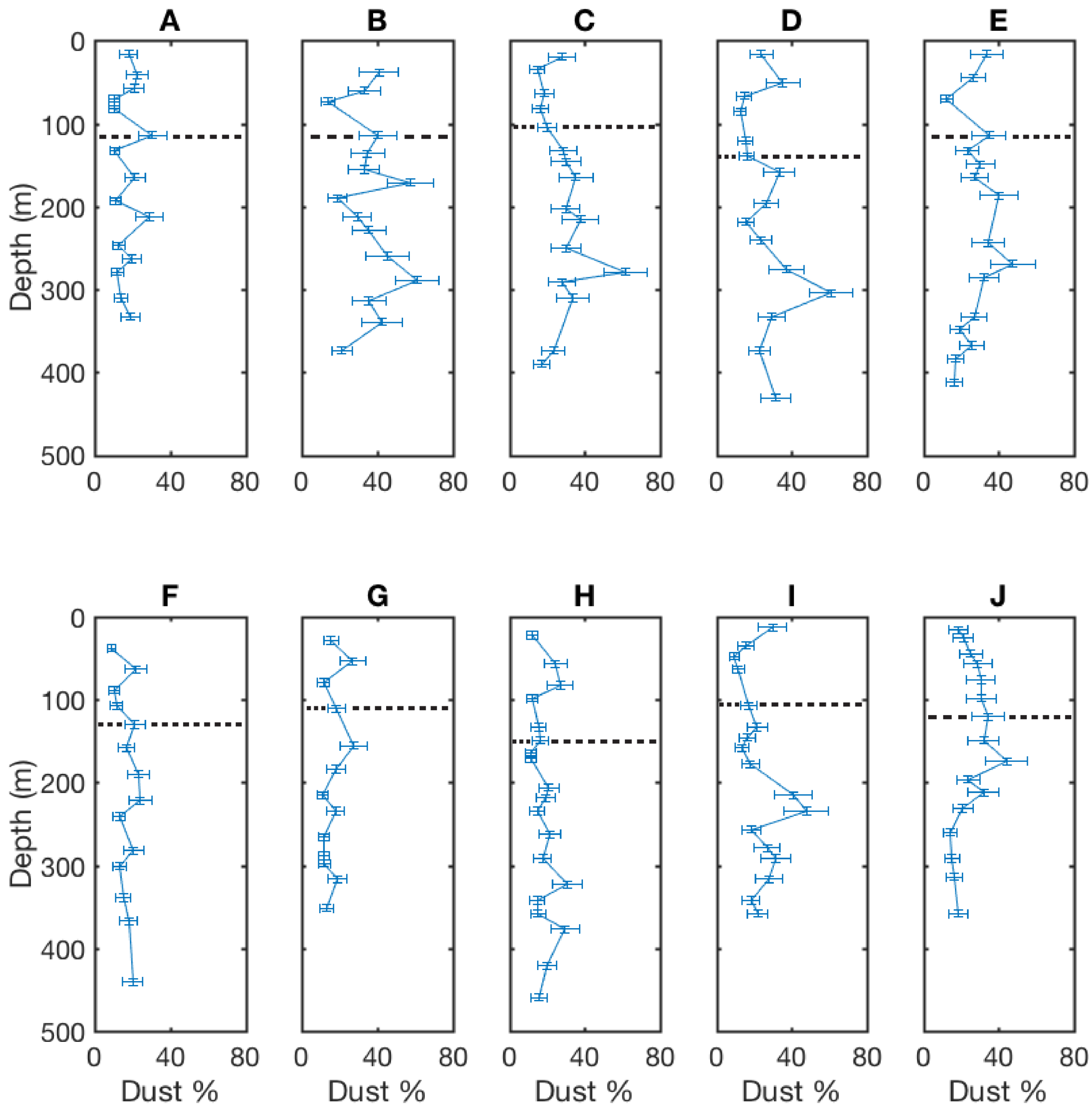

Figure 2.8: Profiles of median fractional dust content vs. depth for each analyzed profile. Vertical error bars are +/- 4.5, in accordance with SHARAD's theoretical resolution in water ice. Horizontal error bars are the standard deviation of the dust distribution for each reflector. Dotted lines mark the cap-wide reflector discussed in the text and shown in Figure 2.3.

While we have been able to constrain the dust content of individual reflectors to a relatively narrow range, there is still noticeable uncertainty in this estimation due to the ambiguity in layer thickness. As shown in Figure 6, there is an excursion in modeled reflectivity toward high dust content values for layer thicknesses between roughly two and four meters. This excursion results in a long tail in each reflector's dust distribution. This leads to an alternate interpretation of reflectivity differences between reflectors. Instead of these reflectivity differences being the result of large changes in dust content, they could instead be smaller fluctuations in layer thickness. This hypothesis was examined in more detail by *Lalich and Holt* [2016]. They concluded that there was superficial correlation between regional radar reflectivity and reflector depth, implying that areas with higher or lower average accumulation rates contained consistently thicker or thinner marker beds, respectively, and this was manifesting in the radar record as variable subsurface reflectivity. However, their work used simplified methods described earlier. Using the full bandwidth model outlined in this work, we see that each layer would have to have a thickness near ~2 or 4 m, where reflectivity is most sensitive to the separation of the layer interfaces, in order for layer thickness variation to explain the differences in reflectivity. *Becerra et al.* [2016] also searched for trends in marker bed thickness with average deposition rates, and found no statistically significant relationship. In addition, multiple studies have identified marker beds with thicknesses well in excess of ~4 m [e.g. *Fishbaugh et al.* 2010b, *Becerra et al.* 2016], meaning that according to our model small variations in their layer thickness would not produce notable changes in reflectivity. Therefore, we favor the hypothesis that the primary cause of reflectivity variation is in fact differences in dust content and not layer thickness.

4.2 Site Variability

As previously noted [*Seu et al.* 2007, *Phillips et al.* 2008, *Lalich and Holt* 2016] there is significant variability in SHARAD reflectivity both geographically and with depth. The mean dust fraction of all reflectors in a given vertical profile shows no correlation with the dust content of the single cap-wide reflector at each site (Table 1). This implies that the processes responsible for the variable composition of this single reflector have likely evolved over the lifetime of the top reflector packet, altering the geographic distribution of ice and dust deposition. This finding indicates that shorter timescale climate events may play just as important a role as orbital cycles determining the composition of NPLD layers.

Mean dust contents between each site vary from 17% to 36%, or slightly over a factor of two. Larger variations can be seen within each site as well. These large variations show the importance of constraining small-scale regional differences in ice and dust deposition in future work, and suggests the use of caution when inferring global climate information from NPLD stratigraphy at a single location.

Site	**A**	**B**	**C**	**D**	**E**
Cap-wide Reflector Dust Content	30%	40%	20%	16%	35%
Mean Dust Content	17%	36%	28%	27%	28%
Site	**F**	**G**	**H**	**I**	**J**
Cap-wide Reflector Dust Content	21%	18%	17%	17%	34%
Mean Dust Content	17%	17%	19%	23%	27%

Table 2.1: Comparison of mean dust content and cap-wide reflector dust content at each study site.

While it is hard to directly compare reflectors without explicitly connecting them through subsurface mapping, trends in dust content with depth do not tend to match from site to site. For example, while sites B, C, and D contain a prominent dusty layer around 300 m depth, the nearby sites E and A do not share this feature. As each profile samples only a small geographic area of the NPLD, this could potentially be the result of smaller scale variations within the larger regional trend. These findings indicate that in order to use SHARAD stratigraphy as a global climate record, one must first carefully consider the local deposition conditions, and how those conditions may have changed through time.

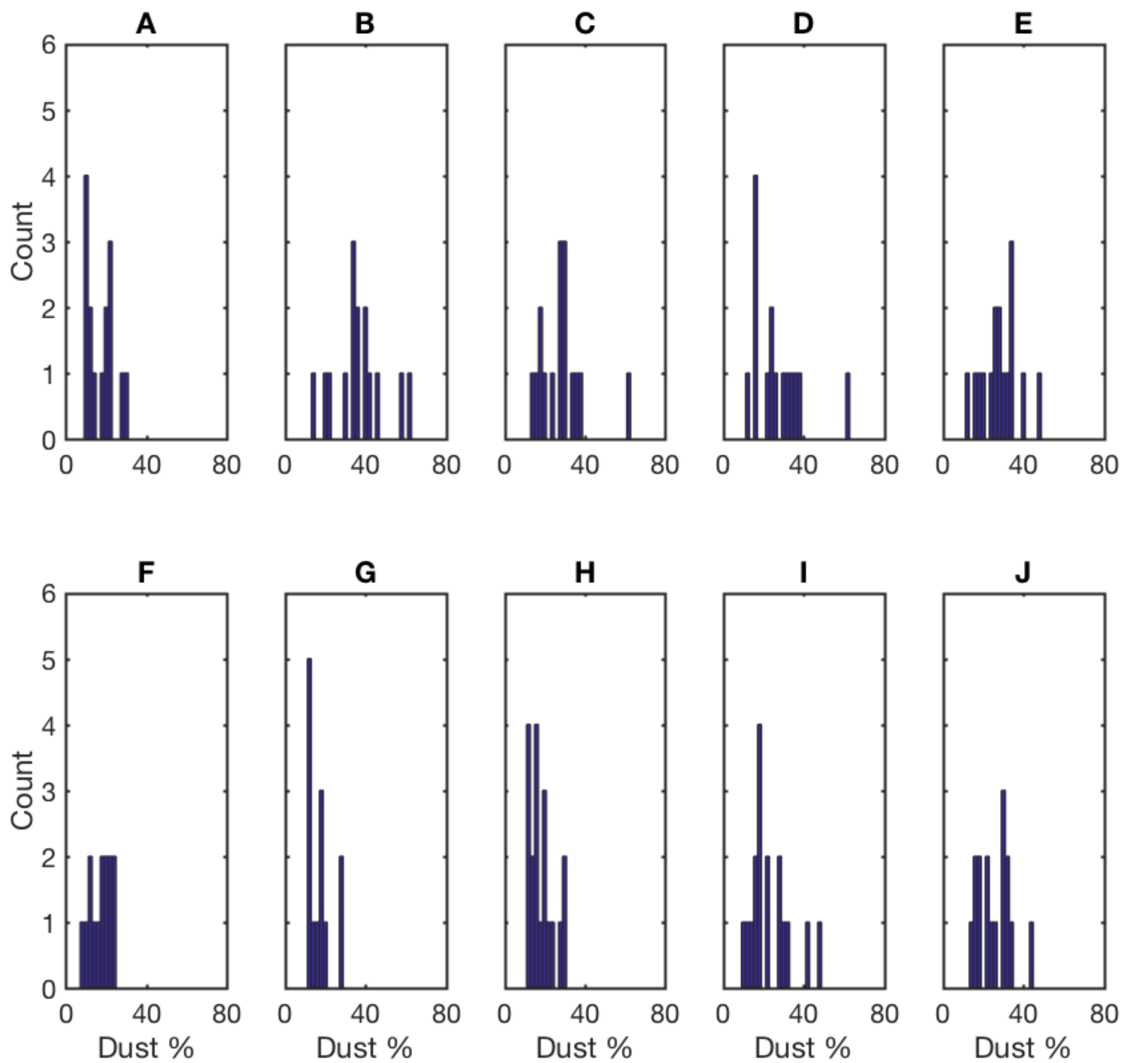

Figure 2.9: Histograms of dust content for each reflector at each study site. Bin sizes are 2%.

It is also notable that the number of reflectors identified at each site is not consistent. Given that the cap-wide reflector discussed here represents an erosional surface [Smith et al. 2016], it is likely that some reflectors at each site are not laterally continuous across the entire cap, and thus do not appear in the record sampled by each profile. Reflectors could also be interfering with each other or be too closely spaced, causing some to go unresolved. This hypothesis is supported by the fact that the profiles with the most reflectors are at sites where the top layer packet is the thickest. This implies that deposition rates were generally higher in these areas during packet accumulation, which could cause reflector-forming layers to be spaced further apart. This extra spacing between layers would make any reflectors they might cause more easily resolvable. Separation distances between reflectors at each site are on the order of ~22-27 m, which is near the estimated reflector separation resolution of 20 m for SHARAD [*Nunes and Phillips* 2006]. This implies that some reflector-forming layers are simply not resolved at each site, as their separation distance falls below this limit. This finding suggests that future work aiming to use radar stratigraphy as a climate record should be conducted where the cap is thickest, in order to ensure that the stratigraphic record is as complete as possible.

4.3 Layer Formation Processes and Climate Model Comparisons

As discussed in section 2.3, previous work has suggested that reflector-causing layers are formed through two main processes, both of which are primarily controlled by the planet's orbital parameters: the concentration of dust through ice sublimation [*Toon et al.* 1980, *Levrard et al.* 2007], or the non-uniform variation of ice and dust deposition with time [e.g. *Cutts and Lewis* 1982, *Phillips et al.* 2008, *Putzig et al.* 2009, *Hvidberg et al.* 2012]. These two processes should result in distinct populations of layers. Lag deposits should consist almost entirely of dust and either empty or ice-filled pore space, while constructional layers should have much lower fractional dust contents, between 3-10% according to a recent model of obliquity-driven polar ice and dust deposition [*Hvidberg et al.* 2012]. However, our dust content estimates do not recreate this bimodal behavior. The full distribution of dust content for analyzed layers is shown in Figure 10. We find only two reflectors for which dust content is less than 10% and only four of the 156 analyzed reflectors have a dust content over 50%. This result does not match either of the proposed layer formation processes.

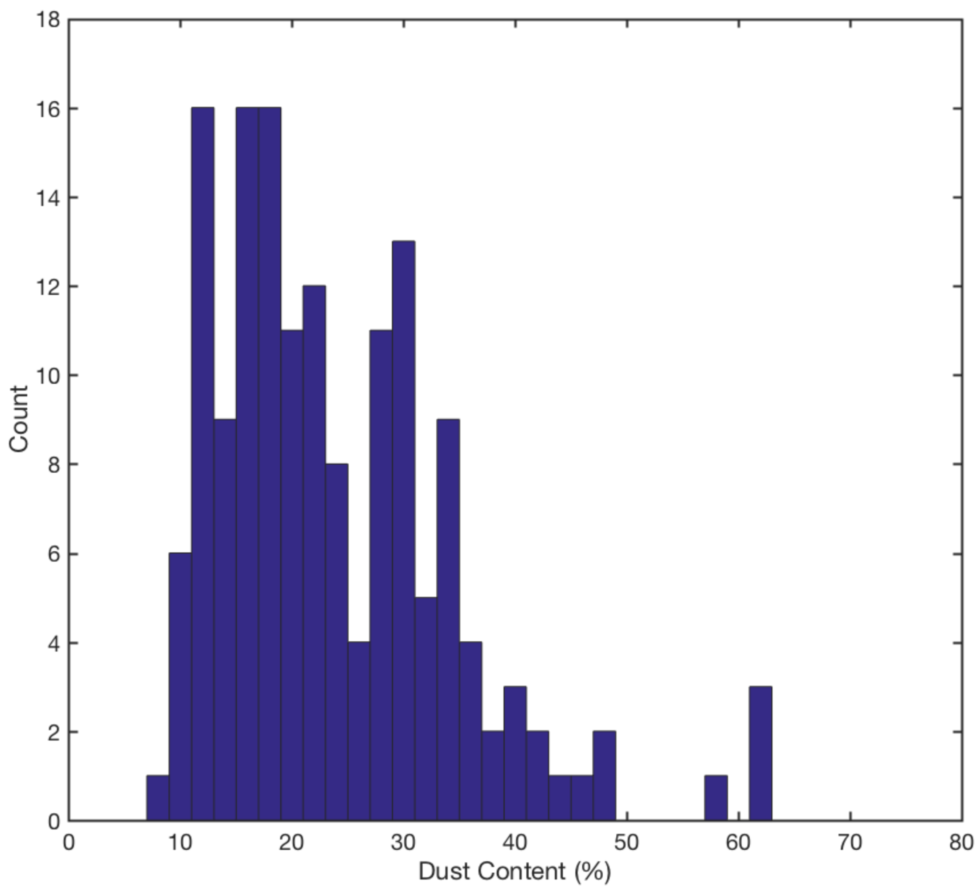

Figure 2.10: Histogram of all estimated dust fractions across all sites. Bin size is 2%.

It is possible that reflectors caused by bright, high dust content layers are masking any reflectors caused by dimmer, low dust content layers that might otherwise be present in the radar record. Bright reflectors are identified at a spacing close to SHARAD's resolution in the upper reflector packet. Any layers with a fractional dust content below 10% that might be between these high dust content layers simply would not be resolved by SHARAD. Even if these low dust content layers exist in the interpacket regions, they may not cause strong enough reflections to be visible above SHARAD's noise background. According to our marker bed reflectivity model, a six-meter thick layer with 5% fractional dust content would have a reflectivity of -34.68 dB. At 400 m below the surface, this would correspond to a reflection power of -46.73 dB, far below SHARAD's nominal noise floor of -40 dB. This is consistent with the accumulation model of *Hvidberg et al.* [2012], where low dust content marker beds are predicted throughout the record, and the packet structure that defines SHARAD stratigraphy is interpreted as the result of layers formed during periods of abnormally low ice deposition or possibly even ablation, such as lag deposits. These low ice deposition layers would only form during periods of maximum obliquity, confining them to specific times in the stratigraphic record, similar to the observed reflector packets.

Explaining the absence of lag deposits in our analyzed reflectors is more difficult. As noted above, only four of 156 analyzed reflectors resulted in estimated dust contents above 50%. The mean dust content for all analyzed reflectors was 23.9% with a standard deviation of 10.8%, far below what one might expect for a dust lag. One possible explanation is that these high-dust layers are not related to lag deposits, and any potential dust lags are simply blown away by surface winds before they have the chance to accumulate or are otherwise not preserved.

However, this would require some other mechanism for creating layers with high fractional dust contents. *Hvidberg et al.* [2012] modeled both dust and ice deposition as anti-correlated with obliquity, i.e. higher obliquity resulted in lower deposition rates, and vice-versa. This created two alternating types of model layers 180 degrees out of phase in the obliquity cycle: those formed during periods of maximum dust deposition, and those formed during periods of minimum ice deposition. However, polar dust deposition rates may not be so simply correlated with obliquity. For example, *Newman et al.* [2005] modeled the dust cycle of Mars under different orbital conditions and found that dust deposition rates increase as obliquity moves further away from 25 degrees, whether that departure is toward higher or lower obliquities. This means dust deposition rates would effectively go through two full cycles of maximum and minimum deposition for each obliquity cycle. Most importantly, this means dust deposition rates would actually be approaching their maximum at the same time the modeled ice deposition rates of *Hvidberg et al.* [2012] are approaching their minimum. Their model placed minimum ice deposition rates on the order of ~0.1 mm/yr and maximum dust deposition rates near ~0.02 mm/yr, which when combined would result in a fractional dust content of ~20%, similar to the values estimated here. In order to determine if this co-varying behavior of ice and dust deposition is a plausible mechanism for creating reflector-causing layers, a better understanding of how the global dust cycle changes over geologic time is necessary.

Another possible explanation for the absence of lag deposits is that any dust lags present on the surface of the cap are somehow mixed with the ice underneath them by winds or other processes before being cemented by further ice deposition. This could include ice diffusing through the lag deposits and filling the pore space. This type of mixing could potentially result in previously nearly pure dust layers being transformed into predominantly water ice layers with higher than average dust contents.

5. Conclusion

We have presented a method for using SHARAD reflection power as a proxy for dust content in the NPLD. By measuring the reflectivity of an individual reflector and comparing it to a model approximating marker bet reflectivity, the range of possible dust contents for the reflector-causing layer can be constrained to a narrow distribution. The impact of layer thickness variation should not be entirely discounted, but evidence suggests dust content is the primary driver of reflector variability.

The mean reflectivity at each of our study sites does not correlate with the local reflectivity of a single cap-wide reflector, indicating changes in the geographic distribution of ice and dust deposition over time. In addition, the number of reflectors identified at each site is not consistent. This is likely a result of well-known erosional unconformities that removed layers, as well as lower average accumulation rates at some sites causing layers to be spaced closer together, thus making them difficult for SHARAD to resolve. These two observations indicate that regional processes play a large role in determining layer properties, and must be carefully accounted for if the NPLD is to be used as a global climate record from orbital-based observations.

Estimates of fractional dust content do not display the expected bimodal distribution described in the literature. Instead, it is possible that low dust content layers that might otherwise cause reflections in the upper reflector packet are simply drowned out by much brighter high-dust reflectors, and while they might be present in the interpacket regions of the NPLD, any reflections they cause are likely too dim for SHARAD to detect at the chosen sites. The presence of dust lag deposits can not be confirmed from our calculations, possibly due to mixing with the surrounding ice prior to cementation or to surface conditions preventing the preservation of such layers. We show that the high dust contents estimated here could instead be explained by altering a previously published NPLD accumulation model, though further work is necessary to confirm this hypothesis.

Chapter 3: Connecting Visible and Radar Stratigraphy in the Martian North Polar Layered Deposits

1. Introduction

The North Polar Layered Deposits (NPLD) of Mars are a quasi-circular formation 1000 km across and between 1.5 and 2 km thick consisting of many sub-parallel layers of water ice and dust that began accumulating approximately 4 million years ago [*Tanaka* 2005, *Levrard et al.* 2007, *Greve et al.* 2010]. This layering is thought to be the result of fluctuations in dust content with depth, possibly as a result of orbital forcing [e.g. *Toon et al.* 1980*, Cutts and Lewis* 1982, *Laskar et al.* 2002, *Levrard et al.* 2007]. Layers are visible at multiple scales in both outcrop imagery and orbital radar sounding data. However, efforts to correlate patterns in either optical stratigraphy or radar stratigraphy to climate conditions have produced mixed results [e.g. *Milkovich and Head* 2005, *Milkovich et al.* 2008, *Perron and Huybers* 2009, *Putzig et al.* 2009, *Hvidberg et al.* 2012, *Becerra et al.* 2017].

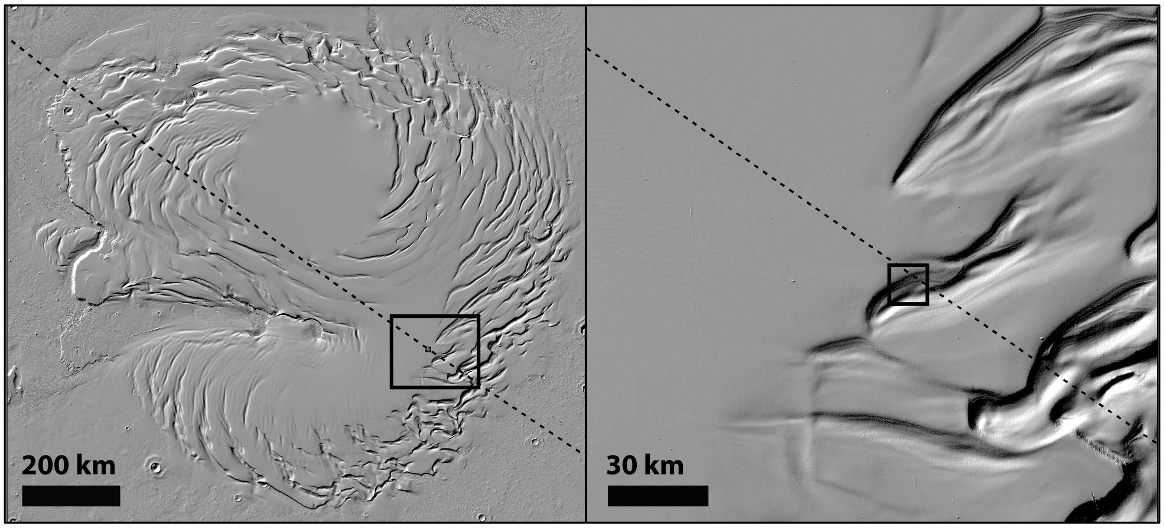

Figure 3.1: Left: MOLA hillshade context map. The dotted line is the approximate ground track for the radargram shown in Figure 3. The black box outlines the area shown on the right. **Right:** Expanded section of the MOLA hillshade map. Dotted line is the same ground track as on the left. The black box shows the approximate footprint of the outcrop image in Figure 2.

Studies of outcrop imagery have been able to link specific layers and sets of layers across the polar cap using morphology, albedo profiles, or high-resolution topography [e.g. *Malin and Edgett* 2001, *Fishbaugh and Hvidberg* 2006, *Milkovich et al.* 2008, *Becerra et al.* 2016]. However, tying these stratigraphic profiles to orbital forcing signals remains a challenge. Previous work identified dominant spatial wavelengths on the order of ~20 – 30 m [*Milkovich and Head* 2005, *Milkovich et al.* 2008]. However, further investigation revealed that this pattern may not be statistically significant, and instead identified a dominant signal at ~1.6 m spatial wavelength, the source of which remains unclear [*Perron and Huybers* 2009]. Other work has suggested that accumulation rates vary considerably across the NPLD, which may make it difficult to identify similar patterns at separate sites [e.g. *Fishbaugh and Hvidberg* 2006, *Becerra et al.* 2016, *Smith et al.* 2016, *Lalich and Holt* 2016, *Lalich et al.* in prep]. To circumvent this issue, recent work has compared a characteristic ratio of periodicities that is present in multiple outcrops to a similar ratio in the insolation record [*Becerra et al.* 2017]. This connection remains somewhat tenuous, however, as the identification of this ratio was inconsistent from outcrop to outcrop.

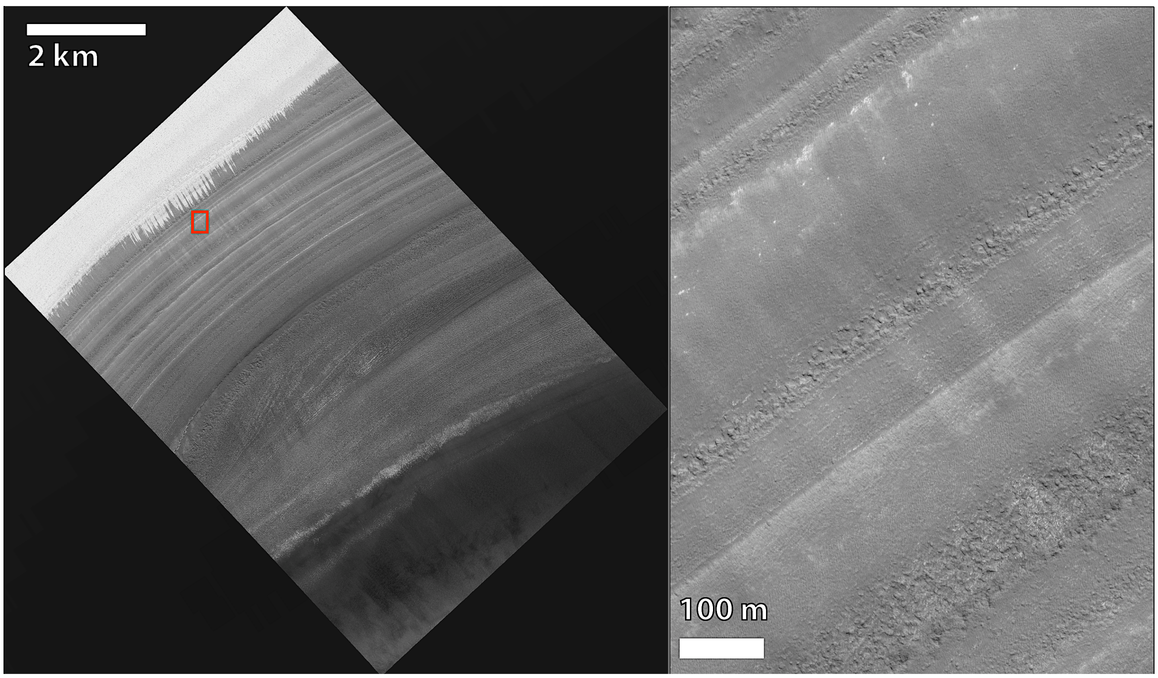

Figure 3.2: Left: HiRISE image ESP_018910_2625 of the trough outcrop used in this study. Red box is the location of the enlarged image on the right. The trough slopes downward the bottom right of the image. **Right:** close-up view of outcrop showing multiple types of layers.

Studies focusing on radar stratigraphy have produced similarly mixed results. Using the Shallow Radar (SHARAD) on the Mars Reconnaissance Orbiter, scientists have identified dozens of sub-parallel reflectors within the NPLD [*Phillips et al.* 2008]. Unlike outcrop imagery, these radar reflectors can be continuously mapped throughout the subsurface, eliminating some of the ambiguity that comes from investigating small-scale sites such as trough walls or other outcrops. These reflectors are organized stratigraphically into four "packets" separated by distinct reflection-free "inter-packet" regions [*Phillips et al.* 2008]. Similar to finer-scale outcrop layering, these reflector packets have been correlated to broad changes in the planet's orbital parameters [*Phillips et al.* 2008, *Putzig et al.* 2009, *Hvidberg et al.* 2012].

However, these correlations are inconclusive, and are difficult to verify without more detailed knowledge of the layers responsible for causing reflectors. Generally speaking, radar reflections are caused by abrupt changes in the electrical permittivity of the subsurface material. Such transitions are commonly found at the interface between two geologic layers of different compositions. In the NPLD, layers of ice with abnormally high dust content are thought to be the primary cause of radar reflections [*Nunes and Phillips* 2006, *Phillips et al.* 2008]. Unfortunately, SHARAD's range resolution (~8.4 m in water ice) is an order of magnitude lower than the available imagery resolution (0.25 – 1.3 m/pixel) [*Seu et al.* 2007, *McEwan et al.* 2007], and layers are visible at scales at least as fine as this higher resolution [*Herkenhoff et al.* 2007]. This makes it difficult to identify which layers cause radar reflectors and what their physical characteristics might be.

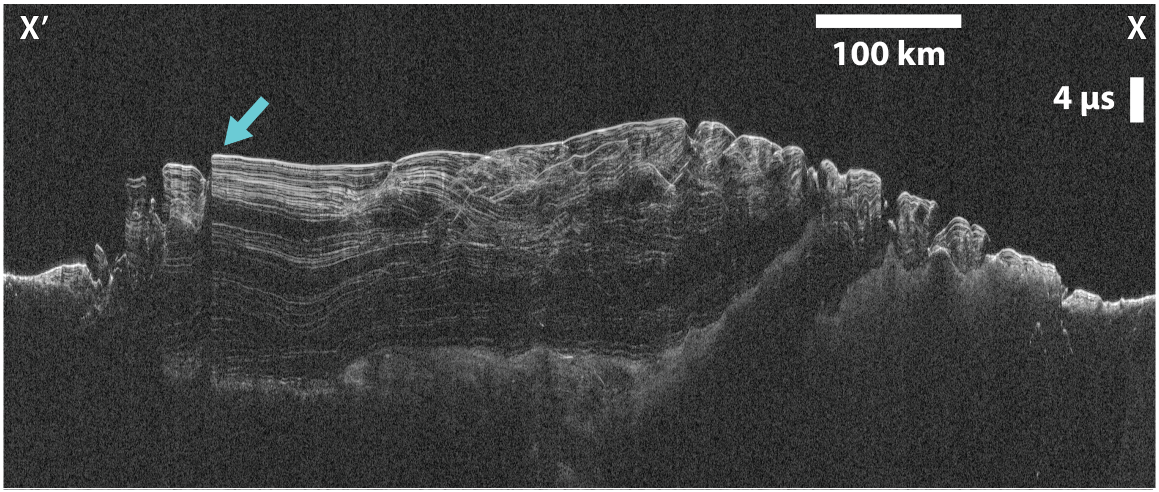

Figure 3.3: SHARAD radargram 1716901000 crossing the entire NPLD. The blue arrow points to the analyzed outcrop.

Some research has attempted to connect optical stratigraphy to radar stratigraphy in an effort to resolve the ambiguities in each dataset. These efforts have focused primarily on the so-called marker beds, which are defined by their relatively strong resistance to ablation compared to surrounding layers [*Malin and Edgett* 2001, *Fishbaugh and Hvidberg* 2006, *Fighbaugh et al.* 2010a, *Christian et al.* 2013]. This resistance implies that these layers are compositionally different from surrounding layers, making them good candidates for the source of radar reflections. Marker beds can be easily identified in high-resolution digital elevation models (DEMs) at scarps and trough walls using protrusion profiles, which are more easily correlated across different outcrops than imagery [*Fishbaugh et al.* 2010a, *Becerra et al.* 2016].

Christian et al. [2013] compared a set of radar observations to a DEM-derived stratigraphic profile of a nearby outcrop, and while they were unable to directly correlate specific radar reflections to specific visible layers, they were able to match dominant periodicities in the radar stratigraphy to similar cyclic behavior in outcrop stratigraphy, suggesting that the two share a genetic link. Further work showed that layers approximating marker beds are capable of producing radar reflections similar to those observed by SHARAD [*Lalich and Holt* 2016], and that it may be possible to infer the dust content of individual layers using radar data [*Lalich et al.* in prep]. Despite this circumstantial evidence, no explicit correlation between individual marker beds and radar reflectors has yet been made. If such a connection could be drawn, it would eliminate much of the uncertainty involved in using either data set as a climate record. Toward that end, we present a comparison of SHARAD radargrams to a high-resolution stratigraphic profile of the upper NPLD, using newly developed radar processing techniques to provide constraints on the thickness of reflector-causing layers.

2. Data and Methods

2.1 Radar Data

SHARAD is an orbital sounder on the Mars Reconnaissance Orbiter (MRO). It uses a chirped signal with a bandwidth of 10 MHz at a center frequency of 20 MHz transmitted over 85 μs [*Seu et al.* 2007]. SHARAD's nominal range resolution is 8.4 m in water ice [*Seu et al.* 2007] though in practice it may not be possible to resolve individual reflectors that are less than ~20 m apart [*Nunes and Phillips* 2006]. Cross-track resolution is between 3-6 km, while along-track resolution of 0.3-1 km is achieved using synthetic aperture processing [*Seu et al.* 2007]. Individual reflectors are traced across multiple observations using intersecting radargrams to confirm that the same reflector is in fact being mapped in each observation. Radargrams are typically recorded and expressed in terms of time delay on their vertical axis. However, the elevation of specific reflectors can be obtained by "depth-correcting" the radargram. This process involves converting the time delay between the surface and subsurface reflections into depth using an assumed dielectric constant for the subsurface material. Here, we assume a dielectric constant of 3.15 for the NPLD, consistent with previous estimates [*Grima et al.* 2009]. This depth below the surface is then converted to elevation by referencing the surface reflection to topographic data collected by the Mars Orbiter Laser Altimeter (MOLA).

As part of this study, we use newly developed "split-chirp" data in addition to normal SHARAD products. Each trace of a SHARAD radargram is retrieved by convolving the reflected signal with the original transmitted signal in the frequency domain in a process known as "pulse compression" [*Seu et al.* 2007]. This process is usually done using the full 10 MHz bandwidth of the transmitted signal, which is known as a "chirp." However, the same technique can be applied using only a portion of the original bandwidth for the convolution. In addition to the typical full-chirp data, we analyze radargrams produced using 5 MHz bandwidths from the high (20 – 25 MHz), low (15 – 20 MHz) and central (17.5 – 22.5 MHz) portions of the full transmitted signal. As the range resolution of the radar is proportional to its frequency bandwidth [*Seu et al.* 2007], split-chirp radargrams have half the resolution of their full-chirp counterparts, i.e. ~16.8 m in water ice. By comparing these products we are able to examine how the same subsurface stratigraphy responds to different frequencies, and we can use that information to place constraints on the physical properties of subsurface layers.

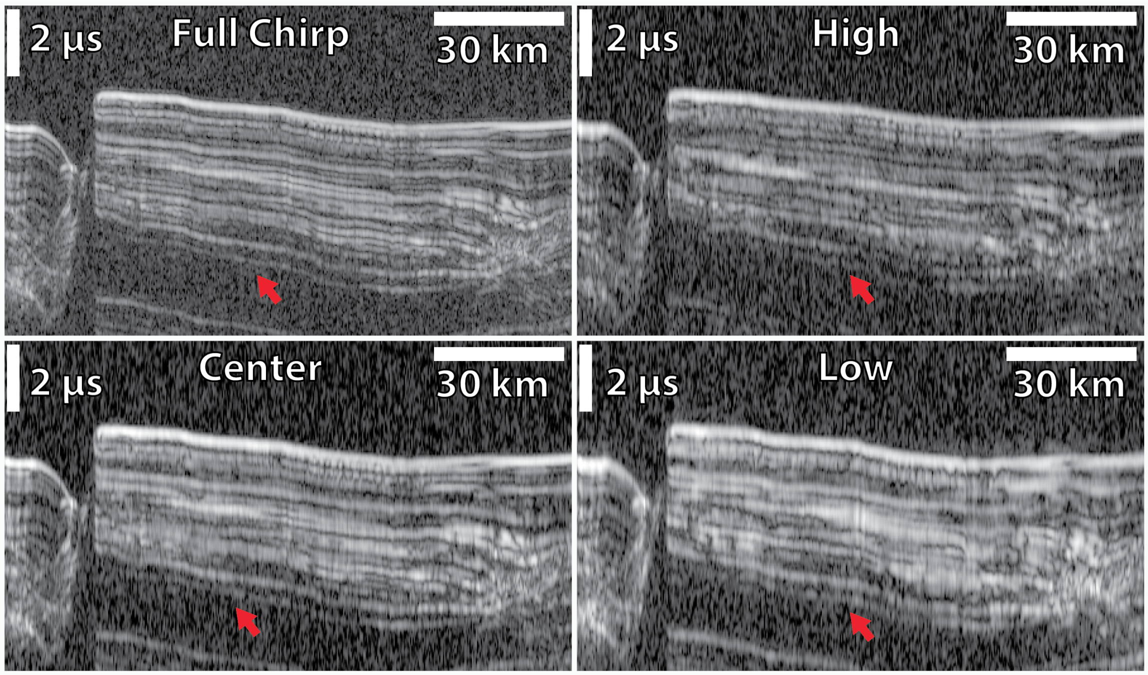

Figure 3.4: Sample radargrams of SHARAD observation 1716901000 showing the same portion of the top reflector packet using the full (15-25 MHz), high (20-25 MHz), center (17.5-22.5 MHz), and low (15-20 MHz) bandwidth portions of the SHARAD chirp. The red arrow indicates the reflector discussed in section 3.3 and marks the approximate location of the traces used for split-chirp reflectivity analysis.

2.2 Study Site

One factor that has hindered previous attempts to correlate radar reflectors with visible layers is observation geometry. In previous work, radargrams intersected the targeted trough wall at an oblique angle. This resulted in the inability to trace reflectors closer than ~10 km to the outcrop DEM [*Christian et al.* 2013]. At this distance, uncertainties in the slope of subsurface reflectors made interpolating their elevations to the trough wall infeasible. In order to account for this issue we chose a study site at 82.4 N, 34.1 E, where SHARAD radargrams intersect the target outcrop at nearly normal incidence. This location in the saddle region of the NPLD is particularly smooth, reducing surface clutter and making subsurface reflectors easier to map continuously. This site also falls within a region that has been previously studied in detail with SHARAD [*Lalich and Holt* 2016, *Lalich et al.* in prep]. Three radargrams were found to pass through the DEM at this site with ideal geometry. In addition to the full-chirp radargrams available on NASA's Planetary Data System, split-chirp data products were created for each observation.

2.3 Layer Morphology, Thickness, and Elevation

The stratigraphic profile of this site was compiled using a combination of high-resolution imagery and a DEM created from stereo images, in a process similar to the method used by Fishbaugh et al. [2010b]. All images were taken by the High Resolution Imaging Science Experiment (HiRISE) camera [*McEwan et al.* 2007], also on MRO. Layers were categorized according to their thickness, protrusion, and morphology. All images have a resolution of ~30 cm per pixel, while the DEM has a horizontal resolution of 1 m per pixel and a vertical resolution of ~30 cm per pixel. After accounting for potential observer error, the uncertainty for all outcrop layer thickness and elevation measurements is ± 1.4 m. Please see Fishbaugh et al. [2010b] for further discussion of this uncertainty.

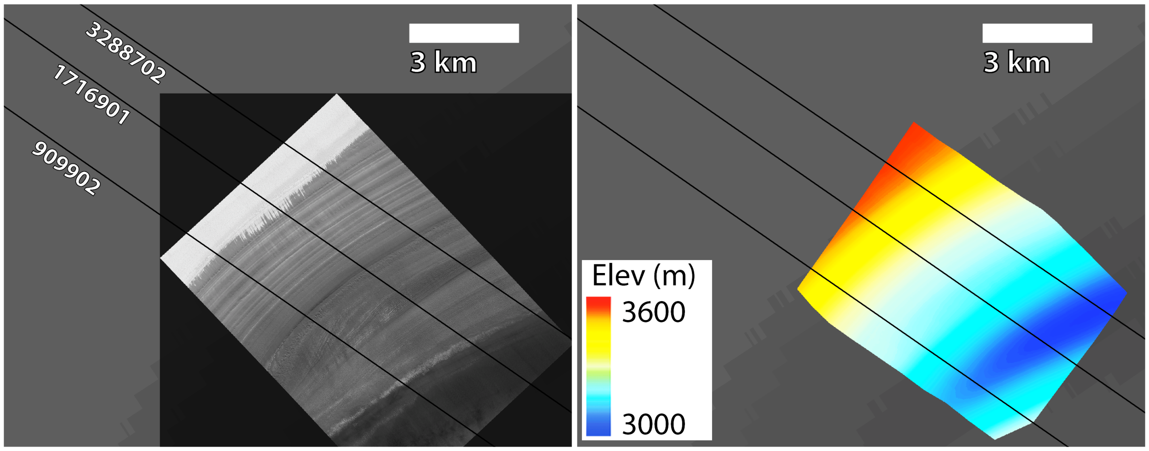

Figure 3.5: Left: Map-projected HiRISE image ESP_018910_2625 with intersecting SHARAD ground tracks labeled by orbit number. **Right:** Same SHARAD ground tracks intersecting the HiRISE-derived DEM of the trough wall.

2.3 Radar Reflectivity Analysis

Previous studies have shown that the total power reflectivity of an individual SHARAD reflector can be measured using the ratio of the subsurface reflection power to the surface reflection power [*Lauro et al.* 2012, *Lalich and Holt* 2016, *Lalich et al.* in prep]. Using this ratio rather than the raw reflection power allows us to compare the relative strength of SHARAD reflectors across different radargrams and data products. Here we adopt the formulation of Lalich et al. [in prep]:

$$R_{ss} = \frac{P_{ss}}{P_s} \frac{R_s e^{2\delta kz}}{(1-R_s)^2} \quad (1)$$

Where R_s and R_{ss} are the surface and subsurface reflectivity, P_s and P_{ss} are the surface and subsurface reflection power, k is the wavenumber, δ is the loss tangent, and z is the reflector depth. R_s and δ are both observationally constrained by previous work [*Grima et al.* 2009, *Grima et al.* 2012]. Using this method we can measure not only the reflectivity of standard SHARAD reflectors, but reflectors from split-chirp radargrams as well.

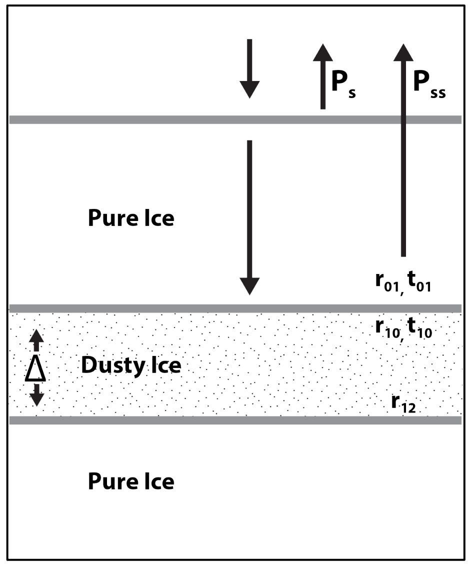

Figure 3.6: Schematic of various measured and modeled parameters necessary for the described reflectivity analysis.

We then compare these observations to a model of marker bed reflection. Because marker beds are thin relative to SHARAD's range resolution, they cannot be modeled as a single, simple interface. Instead, we use the method of MacGregor et al. [2011] to model the reflectivity of a thin, dusty layer approximating a marker bed over a wide range of layer thicknesses and dust contents:

$$R = \left| r_{01} + t_{10} r_{12} t_{01} \left(\frac{e^{-2i\gamma\Delta}}{1 - r_{12} r_{10} e^{-2i\gamma\Delta}} \right) \right|^2 \tag{2}$$

Here, modeled reflectivity (R) is expressed in terms of the Fresnel reflection and transmission coefficients at each interface (r_{xx} and t_{xx} where the first subscript is the layer through which the wave is propagating and the second is the layer it is incident upon, and layer 1 is the dusty layer), the complex propagation constant in the thin layer (γ), and the thickness of that layer (Δ). In order to calculate the necessary Fresnel coefficients, we assume the marker bed layer is surrounded by two layers of pure ice ($\varepsilon_{ice} = 3.15 - 6.3 * 10^{-4}$), and that the dust permittivity is 8.8 – 0.017i [Nunes and Phillips 2006]. We then combine this model with the transmitted SHARAD chirp following the method of Lalich et al. [in prep] in order to produce a model of marker bed reflectivity that accounts for the full frequency bandwidth of SHARAD. This technique involves modeling reflectivity as a function of dust content and layer thickness for each discrete frequency sampled by the transmitted signal, then using the Fourier transform of that signal as an energy density function in order to weight each frequency's contribution to the total reflected power. In addition to the full chirp version of the model, we also produce models of reflectivity as a function of dust content and layer thickness for the high, low, and center frequency bandwidths using the same process.

3. Results and Discussion

3.1 Outcrop Stratigraphy

Using a combination of imagery and the high-resolution DEM we are able to characterize the upper 500 m of the trough wall. The average slope of the trough wall is 4.29 ± 4.64 degrees. Four protrusions interpreted as layers are visible in the upper tens of meters of the DEM, but we are unable to categorize them morphologically as they are obscured by a surface deposit. These layers are between 1.0 and 4.4 ± 1.4 m thick and have an average spacing of 4.4 m. These layers could potentially cause radar reflections, but are spaced too closely together to facilitate tying a specific reflector to a specific layer. If these layers do cause reflectors, it is likely that multiple reflections interfere with each other or otherwise overlap, resulting in reflectors that do not necessarily correspond to single layers but instead to groups of layers.

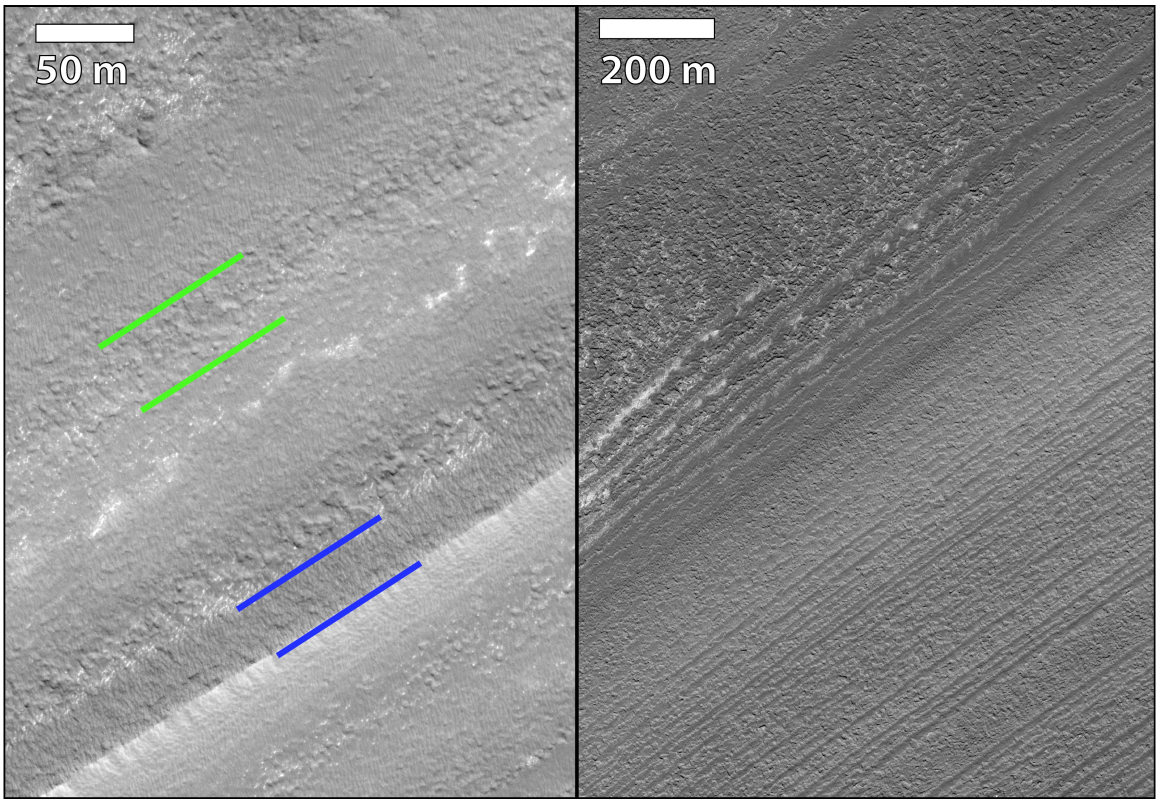

Figure 3.7: Left: Examples of typical pitted layer (green) and marker bed (blue) morphologies. **Right:** Transition from layer sequence characterized by pitted layers and marker beds (top left) to regularly spaced thin layers (bottom right).

The next ~300 meters consist mostly of two types of layers: those matching the description of the original marker bed, and those with a similar step-like relief but smoother surface texture punctuated by scattered pits. These pitted layers are clustered near the top portion of this section, while the more typical marker beds are common near the bottom. The average spacing of layers within this section is 17.9 ± 9 m, and the average layer thickness is 3.9 ± 1.4 m. This spacing is similar to previously reported values for protruding layers at other NPLD outcrops [*Becerra et al.* 2016, *Fighbaugh et al.* 2010b], consistent with the hypothesis that these layers are laterally continuous over much of the polar cap [*Becerra et al.* 2016]. It is unclear whether the pitted layers are intrinsically different from the marker beds or if their different morphologies are the result of surface processes, which are known to obfuscate the expression of outcrop layers [*Herkenhoff et al.* 2007]. Considering their similar separation distances, thicknesses, and protrusions, we conclude that pitted layers and marker beds are the result of similar processes and are likely similar in composition. Most importantly, it is likely that each set of layers is compositionally distinct from the surrounding ice, the primary requirement for generating radar reflectors.

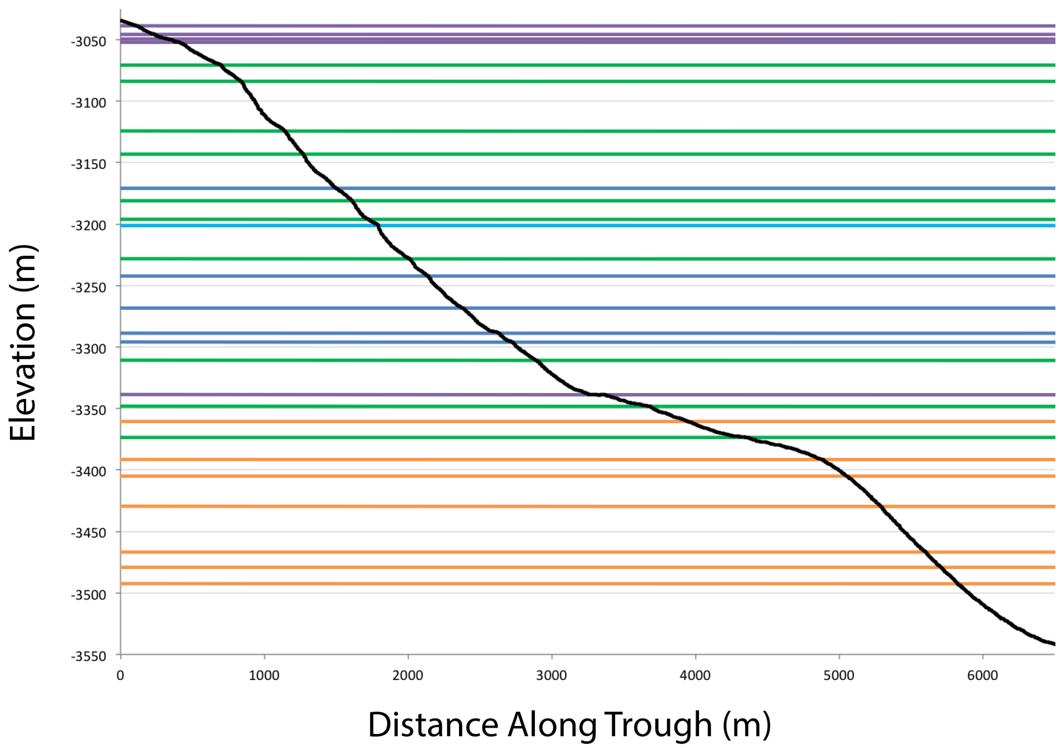

Figure 3.8: Layer elevation plotted over outcrop profile. Purple, green, blue, and orange lines represent unidentified, pitted, marker bed, and prominent thin layers respectively.

The bottom portion of the outcrop profile consists of multiple sets of thin layers, which are on the order of ~1 m thick. Within these packets are individual layers that are prominently expressed in topography and imagery. These prominent layers occur with a nearly regular spacing of approximately 12.5 m, in contrast to the larger and more variable separation distances of the overlying layers, implying that they may be the result of a different forcing mechanism. While these layers could potentially cause radar reflections, their small spacing and thicknesses make correlation with any specific reflector difficult, if not impossible.

Layer Type	Elevation	Thickness
Unknown	-3038.8	4.4

Unknown	-3045.7	2.0
Unknown	-3049.5	1.0
Unknown	-3052.1	3.2
Scattered Pits	-3070.7	4.0
Scattered Pits	-3083.9	4.2
Scattered Pits	-3124.5	2.7
Scattered Pits	-3143.1	2.6
Marker Bed	-3170.9	10.3
Scattered Pits	-3181.0	4.2
Scattered Pits	-3196.2	2.9
Marker Bed	-3201.2	5.8
Scattered Pits	-3228.3	5.0
Marker Bed	-3242.2	3.6
Marker Bed	-3268.3	3.8
Marker Bed	-3288.8	3.6
Marker Bed	-3296.1	3.1
Scattered Pits	-3310.9	3.8
Unknown	-3338.8	5.9
Scattered Pits	-3348.3	3.3
Prominent Thin Layer	-3360.5	1.0
Scattered Pits	-3373.5	2.2
Prominent Thin Layer	-3391.5	1.0
Prominent Thin Layer	-3405.0	1.0
Prominent Thin Layer	-3429.6	1.0
Prominent Thin Layer	-3466.8	1.0
Prominent Thin Layer	-3479.1	1.0
Prominent Thin Layer	-3492.5	1.0

Table 3.1: All prominent protruding layers identified in the trough wall.

3.2 Radar Observations and Comparisons to the Outcrop

Between 17 and 21 reflectors were mapped across the saddle region using each of the three radargrams intersecting the study site. Many of these reflectors are not easily mapped all the way to the outcrop, appearing to merge with other reflectors or ending abruptly tens of kilometers from the trough wall. It is possible that this is the result of pinch-outs or other changes in layer structure, but it is perhaps more likely that this is simply the result of changing layer separation distances and thicknesses, which could cause layers to no longer be resolved as separate reflectors by SHARAD. Previous studies have also observed significant variability in both reflector elevation and reflector strength over relatively small distances [*Christian et al.* 2013, *Lalich and Holt* 2016, *Lalich et al.* in prep], and such changes could explain why each reflector is not observed in each radargram.

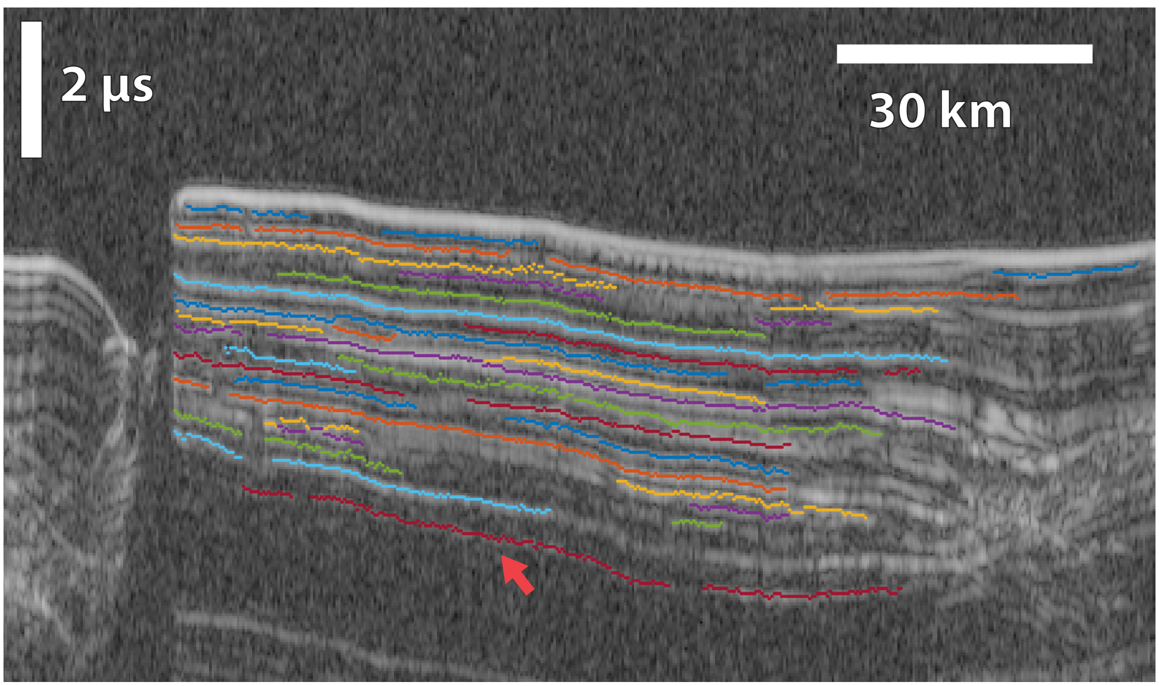

Figure 3.9: SHARAD radargram 1716901000 with mapped reflectors. Note that the vertical axis is time delay, not depth. The red arrow indicates the reflector discussed in section 3.3 and marks the approximate location of the traces used for split-chirp reflectivity analysis.

In contrast to Christian et al. [2013], who had difficulty mapping reflectors within 10 km of their study site due to poor observation geometry, we are able to map multiple reflectors in each radargram within ~500 – 700 meters of the analyzed outcrop DEM.

This allows us to observe features of the subsurface radar stratigraphy that do not appear farther from the trough. Most notably, there is a significant slope break in the radar traces closest to the trough, ~1.5 – 2.0 km from the DEM. While in general reflector slopes are less than 0.1 degrees in magnitude, as they approach the outcrop they increase in magnitude to between -0.4 and -2.4 degrees. This is only observed in the final 2 – 5 traces for each reflector, but it is consistently expressed in each reflector we are able to map close to the outcrop and in all three radargrams.

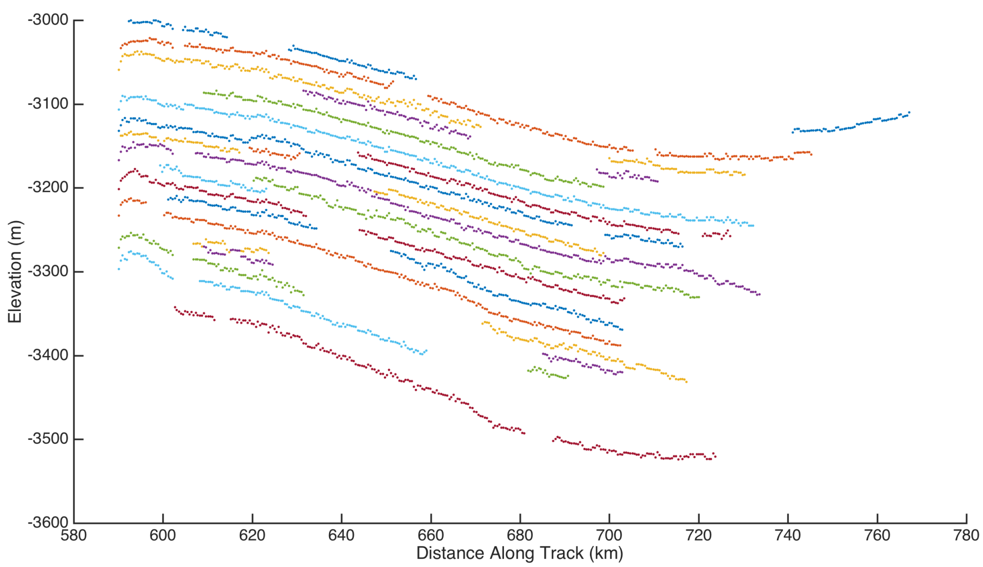

Figure 3.10: Mapped reflectors from Figure 7, depth-corrected and converted to elevation using the MOLA surface for reference and a subsurface dielectric constant of 3.15, consistent with water ice. The x-axis is distance from the first trace of the radargram.

Unfortunately, these steeper slopes complicate attempts to correlate specific reflectors to specific layers. As these steeper, near-outcrop reflector slopes are only expressed over a handful of radar traces, it is difficult to confidently interpolate them all the way to the outcrop. Even if we were to assume the slope calculated from these traces remained constant all the way to the trough wall, the vertical and horizontal uncertainties of SHARAD would result in slope errors on the order of ~1 degree. Because the trough wall itself has a slope of only ~4 degrees, reflectors would need to be interpolated over 1 – 5 km before actually intersecting the surface. Over these distances, the uncertainty in reflector slope corresponds to vertical errors well in excess of 20 m for interpolated radar reflectors, which is greater than the average separation distance between visible layers. Given that this study site contains nearly ideal observation geometry, this result suggests that it may not be possible to make a direct correlation between individual layers and radar reflectors without a higher resolution radar capable of placing tighter constraints on reflector slopes.

While we are unable to connect specific outcrop layers to specific reflectors, we do find some evidence for a common forcing mechanism between the two datasets. The average vertical separation distance for mapped reflectors in each radargram is 17.3 m, 18.5 m, and 21.3 m. Given SHARAD's vertical uncertainty of +/- 4.5 m, these values are indistinguishable from the average separation distance of 17.9 m reported in section 3.1 for the marker beds and pitted layers. These values are also in agreement with dominant spectral features observed at other NPLD outcrops [*Milkovich and Head* 2005, *Christian et al.* 2013, *Becerra et al.* 2017]. While this implies reflector and outcrop layer formation processes are modulated by the same forcing signal, it does not necessarily mean they represent the same paleosurfaces. Instead it is possible that they are responding to the same climate cycle, but are formed at different times. While these consistent separation distances are not conclusive, they do suggest a link between marker beds and radar reflectors.

3.3 Reflectivity Results and Layer Thickness

Reflectivity was calculated for each mapped reflector in the full-chirp radargrams and mean values are reported in Table 2. There is no easily identified trend in reflectivity with depth, but there is significant variability from reflector to reflector, consistent with previous observations [*Lalich and Holt* 2016, *Lalich et al.* in prep]. While reflectivity remains fairly consistent for individual reflectors between all three radargrams, observed values can still vary by ~2 dB for the same reflector. This type of variability is not unexpected, even over such short distances [*Lalich and Holt* 2016], but it is unclear whether this represents real changes in subsurface composition and layer thickness or is instead the result of other errors that have gone unaccounted for.

Full-Chirp Reflectivity (dB) For Each Mapped Reflector

Reflector Number	909902000	1716901000	3288702000
1	-18.69	-22.52	-20.83
2	-18.93	-19.69	-20.32
3	-20.46	-20.25	-21.14
4	-24.18	-23.07	-25.40
5	-24.73	-24.67	-26.74
6	-17.60	-17.94	-19.60
7	-26.28	-25.64	-25.57
8	-18.87	-18.78	-20.34
9	N/A	-17.40	-19.08
10	-16.98	-15.84	-17.08
11	-12.86	-13.71	-14.61
12	N/A	-18.47	N/A
13	N/A	-21.41	N/A
14	-17.87	-16.80	-18.05

15	-18.36	-18.35	-19.30
16	-14.89	-15.33	-15.14
17	-14.21	-14.47	N/A
18	-18.23	-16.54	N/A
19	-20.17	-19.48	-21.56
20	-16.61	-16.23	-17.47
21	-21.86	-21.82	-23.49

Table 3.2: Average full-chirp reflectivity of each mapped reflector in all three radargrams. Reflector numbers correspond to stratigraphic position starting at the surface, i.e. Reflector 1 is the first reflector below the surface. N/A indicates that the given reflector could not be conclusively identified.

Interpreting radar reflectors consistently across split-chirp radargrams is difficult due to their lower resolution. Reflectors are shifted vertically in the high, low, and center bandwidth radargrams, and in places a reflector that is apparent in one frequency band is absent from another. In some cases, what may appear to be a single reflector in one radargram is shown to be two distinct reflectors in another. This is most common when comparing low frequency radargrams to high frequency radargrams. These factors combine to make the positive identification of any single reflector across all radargrams difficult. However, within the three radargrams chosen for this study, we identified a single reflector that was both continuous over a long distance and identifiable in all four data products. The identified reflector was at the bottom of the upper reflector packet, as indicated in Figure 9. This indicates a layer or interface with distinctive properties, and warranted further investigation.

First, in order to measure its reflectivity in the split-chirp products, we chose a 60 trace (~30 km) section from each radargram corresponding to a location where the reflector is identifiable in the high, low, and center frequency band radargrams. We then aligned the surface of each trace and averaged them together, creating one representative reflection power vs. depth profile for each bandwidth. Unfortunately, we were unable to trace this reflector closer than ~35 km from the outcrop. This makes comparisons to outcrop layering difficult, but still allows us to draw broad similarities. A sample profile is shown in Figure 11. In addition to the selected reflector at a depth of ~340 m below the surface, this profile also shows how difficult it can be to interpret reflectors across different parts of the chirp. For example, both the center and low bandwidth radargrams feature a single reflection ~110 m below the surface, but in the high bandwidth radargram, this single reflector is split in two. This implies that the layering responsible for this single reflector in the center and low bandwidth products is more complex than they would otherwise indicate.

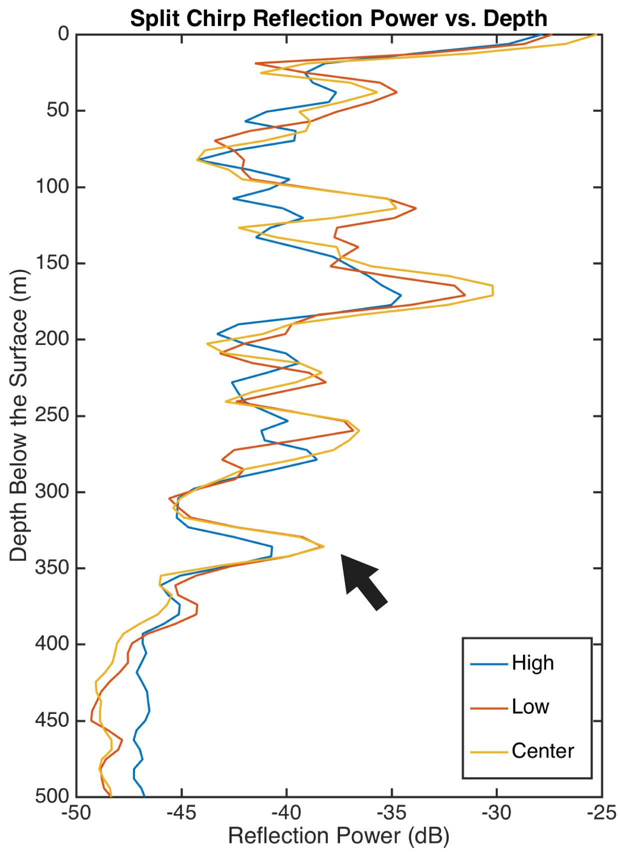

Figure 3.11: Average reflection power profile of the selected section of radargram 1716901000 for each split-chirp bandwidth. Black arrow indicates the reflector chosen for reflectivity analysis.

Reflectivities are measured using the same process applied to the full chirp data. Reflectivities for each bandwidth varied by almost 3 dB between radargrams, an unexpected result given the proximity of each observation. While it is possible that this represents real changes in the subsurface, it is also possible that this is simply a result of noise in the data, especially given the loss of vertical resolution associated with the split-chirp radargrams. It is also possible that our reference chirp does not perfectly mimic the real transmitted chirp, which can undergo small fluctuations due to the changing temperature of the instrument.

Split-Chirp Reflectivity of the Selected Subsurface Reflector (dB)

Bandwidth	909902000	1716901000	3288702000
High	-16.70	-17.15	-17.58
Center	-17.62	-17.99	-19.45
Low	-15.86	-16.66	-18.61

Table 3.3: Split-chirp reflectivity of the selected reflector for each radargram and frequency bandwidth.

In order to interpret these results, we compare the measured reflectivities to models of thin layer reflectivity. As described in section 2, we create models of reflectivity as a function of layer thickness and dust content for each frequency band. Each of the split-chirp models has a lobed structure similar to the single frequency model of Lalich and Holt [2016]. According to these models, thickness changes on the order of ~1 m can cause reflectivity changes close to ~10 dB. This potentially explains the difference in reflectivity for a given bandwidth between the three radargrams, as layer thicknesses have been shown to change over relatively small distance scales in the NPLD [*Becerra et al.* 2016]. Split-chirp reflectivities are also likely influenced by interference from closely spaced or unresolved reflectors, a source of noise that is exacerbated by the relatively poor resolution of the split-chirp radargrams.

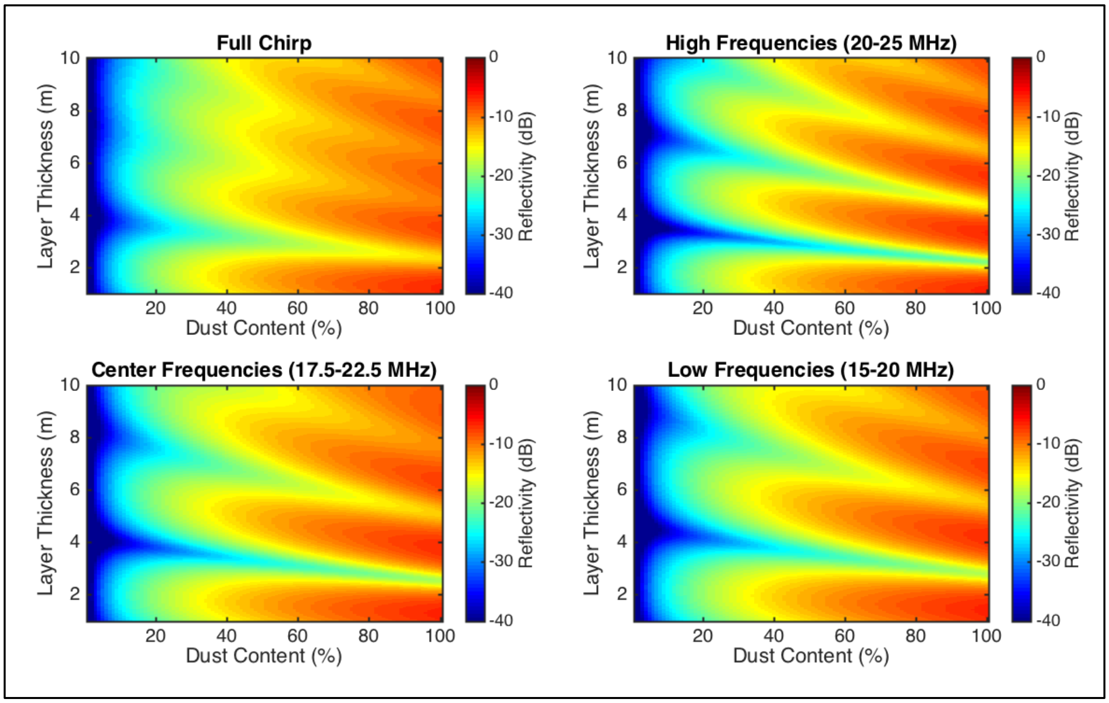

Figure 3.12: Thin layer reflectivity models for the full SHARAD chirp and each frequency band discussed in the text.

As discussed by Lalich et al. [in prep], contours of constant reflectivity are generally constrained to narrow bands of dust content in the full-chirp model. In contrast, contours cover a wide range of both dust content and layer thickness in the split-chirp models. This means that considered individually, they are of limited use for constraining layer properties. However, after taking the difference in reflectivity between two models, (e.g. subtracting the low frequency model from the center frequency model) contours become confined to narrow thickness ranges (Figure 13). Unlike the full chirp case, where reflectivities fall in a single band of dust contents, multiple but distinct layer thicknesses are plausible for any given split-chirp reflectivity difference.

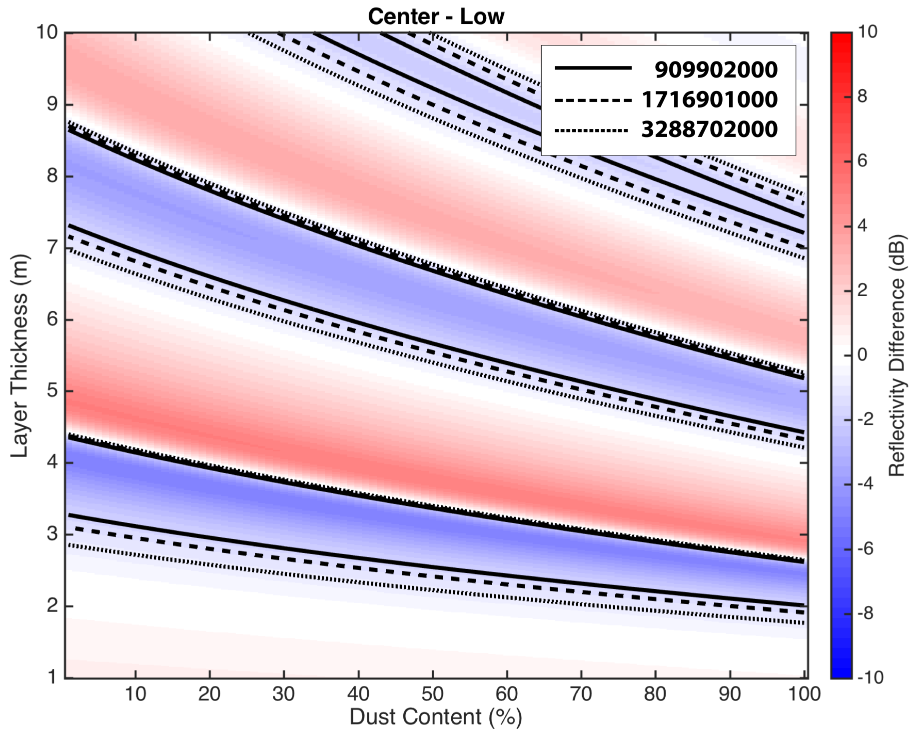

Figure 3.13: Model of the difference in reflectivity between the center and low frequency bands. Contours are the difference in reflectivity between the high and low bandwidth products for the reflector specified in Figure 4.

While this result means it is impossible to use split-chirp radargrams on their own to constrain layer thickness, the potential exists to do so when combined with other types of data. For instance, by comparing the split-chirp reflectivity of a given reflector to its full chirp reflectivity, we can further constrain the layer thicknesses that are likely to produce the observed reflectivities. Figure 14, for example, shows a contour of the average full chirp reflectivity of the analyzed reflector for a single radargram. Contours of the split-chirp reflectivity difference of the same reflector have been plotted on the same axis, and by examining where they intersect the full chirp result we can identify likely layer thicknesses.

These estimates can be further supplemented by the outcrop data. The reflector examined here forms the boundary between a radar-dark interpacket region and the top reflector packet. At its closest mapped proximity to the analyzed outcrop, its elevation is approximately the same as the transition between outcrop layers with marker bed/scattered pit morphologies and thin layer sets, implying that this transition in the outcrop stratigraphy is associated with the transition from packet material to interpacket material. Within the transition region, there is a protruding layer with a thickness of ~3.3 m, which is close to two of the thickness values predicted by the previously mentioned radar observations, near ~3 and 4 m. While this does not prove that the analyzed reflector is caused by this specific outcrop layer, it does mean that such a connection is possible. The correlation of this particular reflector with the transition in the outcrop stratigraphy is particularly noteworthy, as previous work was unable to find any discernable changes in outcrop layers connected to the boundary of the packet and interpacket material as observed in SHARAD radargrams [*Smith et al.* 2015].

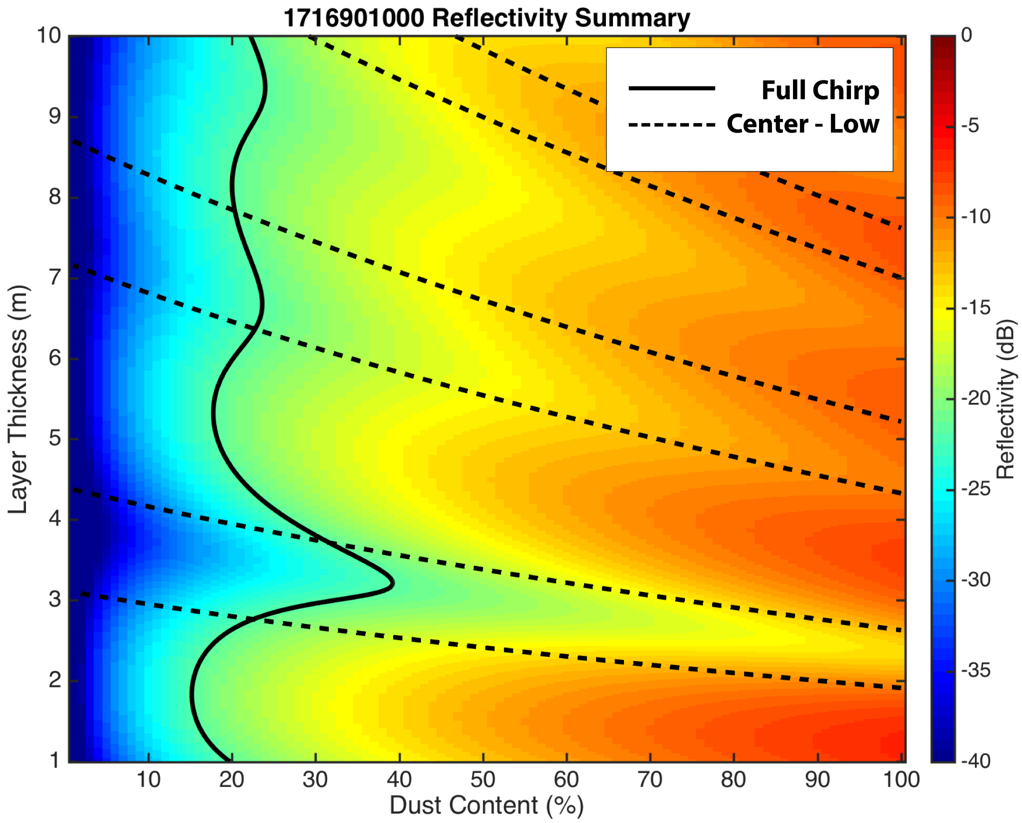

Figure 3.14: Model with reflectivity contours for radargram 1716901000. The color axis is for full chirp reflectivity. The solid line is the contour for the full chirp reflectivity of the reflector discussed in section 3.3 and denoted by red arrows in Figures 4 and 9. Dashed lines are the same as Figure 13, reproduced here to show where they intersect the full-chirp data.

The thickness of this layer also corresponds to a distinctive feature in the full-chirp reflectivity model. In general, reflectivity contours are confined to narrow bands of dust content in the full-chirp model. This observation led Lalich et al. [in prep] to conclude that variations in reflectivity across the NPLD are likely the cause of changes in layer composition rather than thickness. However, they also noted that there is a region in the model's parameter space where the opposite might be true. Between layer thicknesses of ~2 – 4 m, much lower reflectivity values are predicted at higher dust contents compared to the rest of the model. This feature is sharply defined, especially at higher dust contents, so any layer with a thickness in this range could experience large changes in reflectivity due to relatively minor changes in layer thickness. Both the outcrop measurements presented here and the previously discussed split-chirp reflectivity observations imply layer thicknesses near 3 - 4 m in this region of the NPLD, meaning that previously observed variation in SHARAD reflectivity [*Lalich and Holt* 2016, *Lalich et al.* in prep] could in fact be due to small changes in layer thickness rather than large changes in dust content.

Without the investigation of other sites around the polar cap, it is impossible to state definitively whether or not most reflectivity variations are due to changes in layer thickness. This is especially true given that previous studies have measured marker bed thicknesses well in excess of 4 m [*Fishbaugh et al.* 2010a, *Fishbaugh et al.* 2010b, *Becerra et al.* 2016]. It is possible that in some regions layer thickness is the primary cause of deviation, while in others dust content is the more important factor. When examining a cap-wide reflector previously mapped by Smith et al. [2016], Lalich et al. [in prep] found that its reflectivity was consistently lower near the NPLD margins and near troughs. These are areas where changes in layer thickness are likely due to variations in accumulation, but where it is unclear what compositional changes, if any, should be expected. Cap-wide mapping of additional reflectors is necessary to confirm that this trend is consistent, but it suggests that overall, layer thickness variation is most responsible for large-scale geographic changes in SHARAD reflectivity. This could mean that radar reflectivity is acting as a proxy for total accumulation rate in addition to dust content, as previously discussed by Lalich and Holt [2016].

4. Conclusions

Using a combination of high-resolution imagery and topography at an NPLD outcrop, we identified protruding layers with traditional marker bed morphology as well as those with a smoother, pitted surface. When considered together, these layers have similar thicknesses and separation distances to previously analyzed outcrops [*Milkovich and Head* 2005, *Fishbaugh et al.* 2010b, *Becerra et al.* 2016]. Below these layers, we identified sets of thin layers that repeat with a very regular spacing. The elevation of the transition to these layer sets as well as comparisons to radar observations indicate that this thin-layer-set section of the outcrop may represent non-reflective interpacket material.

In an effort to unify this outcrop stratigraphy with radar stratigraphy, we mapped 20 reflectors across three radargrams intersecting the outcrop. While we were able to map reflectors to within 500 m of the trough wall, large uncertainties in reflector elevation and slope made interpolating reflectors to the outcrop impossible to the accuracy required to make unique correlations between reflectors and either single layers or thin layer sets. Given the favorable orbital geometry of this site, we find it unlikely that such an effort would be successful elsewhere without higher resolution radar data, pointing to potential future missions to answer this question. Despite the inability to match specific reflectors to specific layers, we do find evidence for a connection between the two stratigraphies.

Radar reflectors have a vertical spacing consistent with the spacing of outcrop layers, suggesting that their formation is controlled by the same forcing mechanism.

Reflectivity analysis of the full-chirp radargrams revealed no consistent pattern with depth, and while there was close agreement in the reflectivity of individual reflectors across different radargrams, there was still some variability, consistent with previous work [*Lalich and Holt* 2016, *Lalich et al.* in prep]. Examination of split-chirp radargrams found that they are difficult to interpret in the upper layer packet of the NPLD due to low resolution, and may be best applied to areas where reflectors are not so closely spaced. Reflectivity analysis of a single reflector across all three radargrams and frequency bandwidths showed that split-chirp data can not be used to determine layer thickness on its own, but when combined with other observations it can serve to rule out possible thickness values.

Possible values for layer thickness determined from the split-chirp radargrams were consistent with the thickness of an outcrop layer at a similar elevation and stratigraphic transition. This layer thickness also corresponds to a region in the full-chirp reflectivity model's parameter space where small changes in layer thickness can result in large changes in reflectivity. When combined with previous work [*Lalich and Holt* 2016, *Lalich et al.* in prep], this result implies that the observed geographic variability in radar reflectivity may be due primarily to changes in layer thickness, and that this variability could possibly be used as a proxy for relative accumulation rates across the NPLD.

Conclusion

By integrating multiple techniques and data sets, I have shown that it is possible to place quantitative constraints on the global ice and dust cycles of Mars and how they have varied through time. I have also provided evidence that reflections visible in SHARAD orbital radar sounding data are likely caused by layers commonly known as marker beds, helping to unify two previously separate stratigraphic records. These achievements represent a significant step forward in the study of the Martian paleoclimate and the construction of the NPLD.

In the first chapter, I showed that thin dust-rich layers known as marker beds could plausibly produce reflectors with reflectivities similar to those observed by SHARAD. I also showed that there was significant variation in SHARAD reflectivity across the NPLD, an unexpected result that indicates the importance of local processes in forming the polar cap. Finally, I presented the hypothesis that SHARAD reflectivity could be used to track changes in ice and dust deposition rates through time, and that previous work had under-predicted the amount of dust present in individual NPLD layers.

In the second chapter, I showed how SHARAD reflectivity could be used to narrowly constrain the dust content of marker beds. The resulting values for dust content led to the conclusion that radar reflectors are likely not the result of lag deposits, as some previously assumed. At the same time, I showed that previous conceptualizations of how the Martian dust cycle varies over orbital time scales may not be sufficient to explain observations. I also showed that while some regional trends in SHARAD reflectivity may be constant through time, others are not, again indicating that local processes are more important than previously assumed. This further underscored the need to choose study sites carefully and to consider the local context when using the NPLD as a global climate record.

In the third chapter, I showed that outcrop layering and SHARAD reflectors are likely responding to the same forcing signal. By combining a detailed analysis of outcrop stratigraphy with newly developed radar processing techniques, I was also able to show how previously observed variation in SHARAD reflectivity may be caused by changes in layer thickness, and that these variations could be used to track changes in accumulation rates through time.

While many questions remain unanswered, the work presented in this dissertation provides a solid foundation from which to approach them. For the first time, scientists are no longer limited to broad correlations between the stratigraphic record and the Martian paleoclimate. Using the techniques and results presented here, researchers can finally begin to utilize the NPLD as a global climate record, using individual layers to investigate how the ice and dust cycles of Mars have changed over time at a previously unachievable level of detail.

References

Becerra, P., S. Byrne, M. M. Sori, S. Sutton, and K. E. Herkenhoff (2016), Stratigraphy of the north polar layered deposits of Mars from high-resolution topography, *J. Geophys. Res. Planets*, *121*(8), 2015JE004992, doi:10.1002/2015JE004992.

Becerra, P., M. M. Sori, and S. Byrne (2017), Signals of astronomical climate forcing in the exposure topography of the North Polar Layered Deposits of Mars, *Geophys. Res. Lett.*, *44*(1), 2016GL071197, doi:10.1002/2016GL071197.

Brown, A. J., W. M. Calvin, P. Becerra, and S. Byrne (2016), Martian north polar cap summer water cycle, *Icarus*, *277*, 401–415, doi:10.1016/j.icarus.2016.05.007.

Christian, S., J. W. Holt, S. Byrne, and K. E. Fishbaugh (2013), Integrating radar stratigraphy with high resolution visible stratigraphy of the north polar layered deposits, Mars, *Icarus*, *226*(2), 1241–1251, doi:10.1016/j.icarus.2013.07.003.

Cutts, J. A., and B. H. Lewis (1982), Models of climate cycles recorded in Martian polar layered deposits, *Icarus*, *50*(2–3), 216–244, doi:10.1016/0019-1035(82)90124-5.

Fishbaugh, K. E., and C. S. Hvidberg (2006), Martian north polar layered deposits stratigraphy: Implications for accumulation rates and flow, *Journal of Geophysical Research: Planets*, *111*(E6), doi:10.1029/2005JE002571.

Fishbaugh, K. E., S. Byrne, K. E. Herkenhoff, R. L. Kirk, C. Fortezzo, P. S. Russell, and A. McEwen (2010a), Evaluating the meaning of "layer" in the martian north polar layered deposits and the impact on the climate connection, *Icarus*, *205*(1), 269–282, doi:10.1016/j.icarus.2009.04.011.

Fishbaugh, K. E., C. S. Hvidberg, S. Byrne, P. S. Russell, K. E. Herkenhoff, M. Winstrup, and R. Kirk (2010b), First high-resolution stratigraphic column of the Martian north polar layered deposits, *Geophys. Res. Lett.*, *37*(7), L07201, doi:10.1029/2009GL041642.

Garnett, J. C. M. (1906), Colours in Metal Glasses, in Metallic Films, and in Metallic Solutions. II, *Philosophical Transactions of the Royal Society of London. Series A, Containing Papers of a Mathematical or Physical Character*, *205*, 237–288.

Greve, R., B. Grieger, and O. J. Stenzel (2010), MAIC-2, a latitudinal model for the Martian surface temperature, atmospheric water transport and surface glaciation, *Planetary and Space Science*, *58*(6), 931–940, doi:10.1016/j.pss.2010.03.002.

Grima, C., W. Kofman, J. Mouginot, R. J. Phillips, A. Hérique, D. Biccari, R. Seu, and M. Cutigni (2009), North polar deposits of Mars: Extreme purity of the water ice, *Geophysical Research Letters*, *36*, 03203, doi:10.1029/2008GL036326.

Grima, C., W. Kofman, A. Herique, R. Orosei, and R. Seu (2012), Quantitative analysis of Mars surface radar reflectivity at 20 MHz, *Icarus*, *220*(1), 84–99, doi:10.1016/j.icarus.2012.04.017.

Herkenhoff, K. E., and J. J. Plaut (2000), Surface Ages and Resurfacing Rates of the Polar Layered Deposits on Mars, *Icarus*, *144*, 243–253, doi:10.1006/icar.1999.6287.

Herkenhoff, K. E., S. Byrne, P. S. Russell, K. E. Fishbaugh, and A. S. McEwen (2007), Meter-Scale Morphology of the North Polar Region of Mars, *Science*, *317*, 1711, doi:10.1126/science.1143544.

Hofstadter, M. D., and B. C. Murray (1990), Ice sublimation and rheology: Implications for the Martian polar layered deposits, *Icarus*, *84*(2), 352–361, doi:10.1016/0019-1035(90)90043-9.

Hvidberg, C. S., K. E. Fishbaugh, M. Winstrup, A. Svensson, S. Byrne, and K. E. Herkenhoff (2012), Reading the climate record of the martian polar layered deposits, *Icarus*, *221*(1), 405–419, doi:10.1016/j.icarus.2012.08.009.

Lalich, D. E., and J. W. Holt (2016), New Martian climate constraints from radar reflectivity within the north polar layered deposits, *Geophys. Res. Lett.*, 2016GL071323, doi:10.1002/2016GL071323.

Landis, M. E., S. Byrne, I. J. Daubar, K. E. Herkenhoff, and C. M. Dundas (2016), A revised surface age for the North Polar Layered Deposits of Mars, *Geophys. Res. Lett.*, *43*(7), 2016GL068434, doi:10.1002/2016GL068434.

Laskar, J., B. Levrard, and J. F. Mustard (2002), Orbital forcing of the martian polar layered deposits, *Nature*, *419*, 375–377.

Lauro, S. E., E. Mattei, F. Soldovieri, E. Pettinelli, R. Orosei, and G. Vannaroni (2012), Dielectric constant estimation of the uppermost Basal Unit layer in the martian Boreales Scopuli region, *Icarus*, *219*(1), 458–467, doi:10.1016/j.icarus.2012.03.011.

Levrard, B., F. Forget, F. Montmessin, and J. Laskar (2007), Recent formation and evolution of northern Martian polar layered deposits as inferred from a Global Climate Model, *Journal of Geophysical Research: Planets*, *112*(E6), doi:10.1029/2006JE002772.

MacGregor, J. A., S. Anandakrishnan, G. A. Catania, and D. P. Winebrenner (2011), The grounding zone of the Ross Ice Shelf, West Antarctica, from ice-penetrating radar, *Journal of Glaciology*, *57*(205), 917–928, doi:10.3189/002214311798043780.

Malin, M. C., and K. S. Edgett (2001), Mars Global Surveyor Mars Orbiter Camera: Interplanetary cruise through primary mission, *J. Geophys. Res.*, *106*(E10), 23429–23570, doi:10.1029/2000JE001455.

Mattei, E., S. E. Lauro, G. Vannaroni, B. Cosciotti, F. Bella, and E. Pettinelli (2014), Dielectric measurements and radar attenuation estimation of ice/basalt sand mixtures as martian Polar Caps analogues, *Icarus*, *229*, 428–433, doi:10.1016/j.icarus.2013.10.017.

McEwen, A. S. et al. (2007), Mars Reconnaissance Orbiter's High Resolution Imaging Science Experiment (HiRISE), *J. Geophys. Res.*, *112*(E5), E05S02, doi:10.1029/2005JE002605.

Milkovich, S. M., and J. W. Head (2005), North polar cap of Mars: Polar layered deposit characterization and identification of a fundamental climate signal, *Journal of Geophysical Research: Planets*, *110*(E1), doi:10.1029/2004JE002349.

Milkovich, S. M., J. W. Head III, and G. Neukum (2008), Stratigraphic analysis of the northern polar layered deposits of Mars: Implications for recent climate history, *Planetary and Space Science*, *56*(2), 266–288, doi:10.1016/j.pss.2007.08.004.

Newman, C. E., S. R. Lewis, and P. L. Read (2005), The atmospheric circulation and dust activity in different orbital epochs on Mars, *Icarus*, *174*(1), 135–160, doi:10.1016/j.icarus.2004.10.023.

Nunes, D. C., and R. J. Phillips (2006), Radar subsurface mapping of the polar layered deposits on Mars, *Journal of Geophysical Research (Planets)*, *111*, doi:10.1029/2005JE002609.

Nunes, D. C., S. E. Smrekar, B. Fisher, J. J. Plaut, J. W. Holt, J. W. Head, S. J. Kadish, and R. J. Phillips (2011), Shallow Radar (SHARAD), pedestal craters, and the lost Martian layers: Initial assessments, *Journal of Geophysical Research: Planets*, *116*(E4), doi:10.1029/2010JE003690.

Perron, J. T., and P. Huybers (2009), Is there an orbital signal in the polar layered deposits on Mars?, *Geology*, *37*(2), 155–158, doi:10.1130/G25143A.1.

Phillips, R. J. et al. (2008), Mars North Polar Deposits: Stratigraphy, Age, and Geodynamical Response, *Science*, *320*(5880), 1182–1185, doi:10.1126/science.1157546.

Putzig, N. E., R. J. Phillips, B. A. Campbell, J. W. Holt, J. J. Plaut, L. M. Carter, A. F. Egan, F. Bernardini, A. Safaeinili, and R. Seu (2009), Subsurface structure of Planum Boreum from Mars Reconnaissance Orbiter Shallow Radar soundings, *Icarus*, *204*(2), 443–457, doi:10.1016/j.icarus.2009.07.034.

Putzig, N. E., R. J. Phillips, B. A. Campbell, J. J. Plaut, J. W. Holt, F. Bernardini, A. F. Egan, and I. B. Smith (2016), Custom SHARAD Processing via the CO-SHARPS Processing Boutique, *47th Lunar and Planetary Science Conference*, abstract 3010.

Seu, R. et al. (2007), SHARAD sounding radar on the Mars Reconnaissance Orbiter, *Journal of Geophysical Research (Planets)*, *112*, doi:10.1029/2006JE002745.

Skorov, Y. V., W. J. Markiewicz, A. T. Basilevsky, and H. U. Keller (2001), Stability of water ice under a porous nonvolatile layer: implications to the south polar layered deposits of Mars, *Planetary and Space Science*, *49*(1), 59–63, doi:10.1016/S0032-0633(00)00121-5.

Smith, I. B., and J. W. Holt (2015), Spiral trough diversity on the north pole of Mars, as seen by Shallow Radar (SHARAD), *J. Geophys. Res. Planets*, *120*(3), 2014JE004720, doi:10.1002/2014JE004720.

Smith, I. B., N. E. Putzig, J. W. Holt, and R. J. Phillips (2016), An ice age recorded in the polar deposits of Mars, *Science*, *352*(6289), 1075–1078, doi:10.1126/science.aad6968.

Tanaka, K. L. (2005), Geology and insolation-driven climatic history of Amazonian north polar materials on Mars, *Nature*, *437*, 991–994, doi:10.1038/nature04065.

Toon, O. B., J. B. Pollack, W. Ward, J. A. Burns, and K. Bilski (1980), The astronomical theory of climatic change on Mars, *Icarus*, *44*(3), 552–607, doi:10.1016/0019-1035(80)90130-X.